THE STATE OF THE CLIMATE 2021

Ole Humlum

The Global Warming Policy Foundation
Report 51

The State of the Climate 2021
Ole Humlum
Report 51, The Global Warming Policy Foundation

About the author

Ole Humlum is former Professor of Physical Geography at the University Centre in Svalbard, Norway, and Emeritus Professor of Physical Geography, University of Oslo, Norway.

Contents

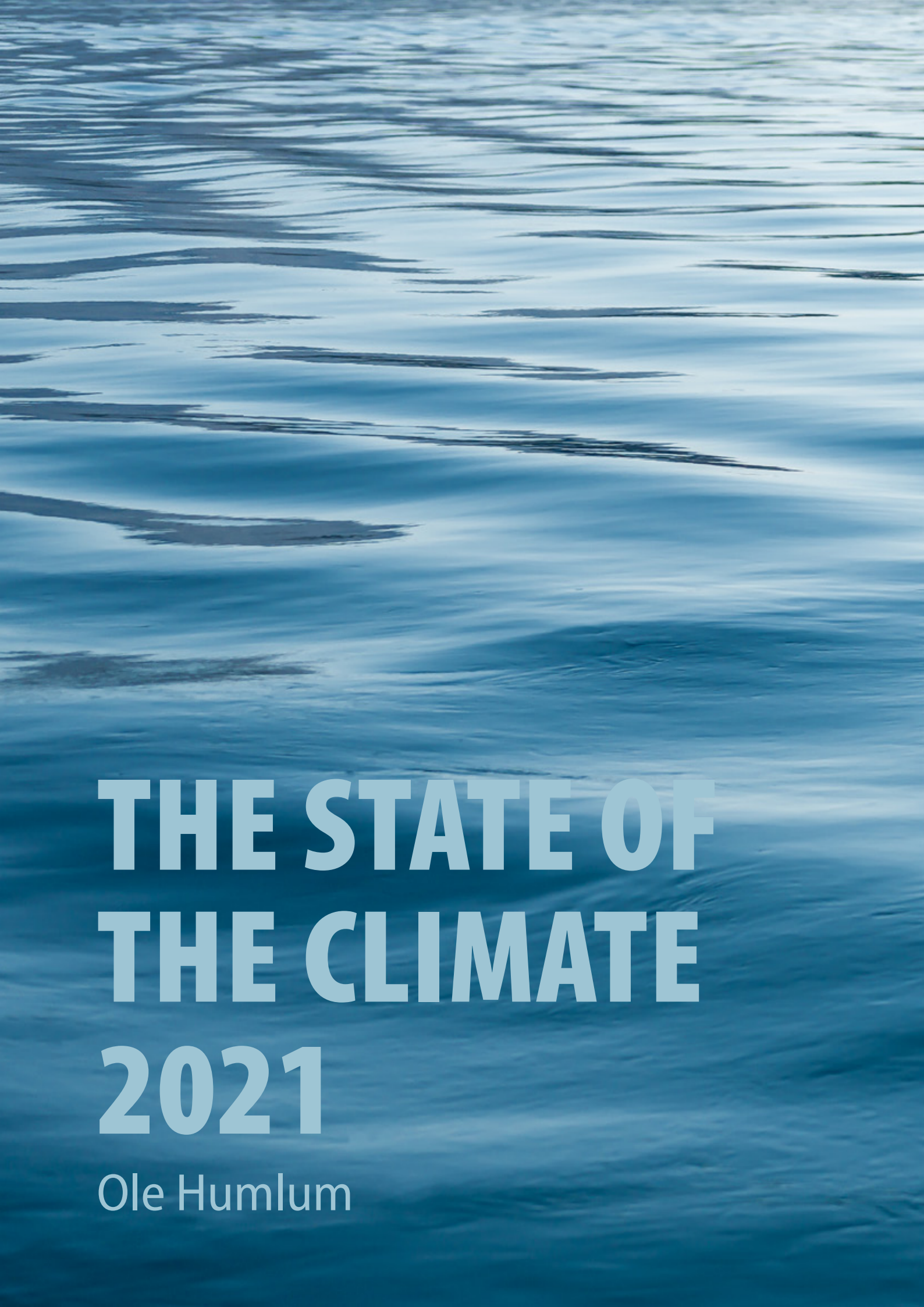

THE STATE OF THE CLIMATE 2021

Ole Humlum

General overview 2021

This report has its main focus on observations and not on the output of numerical models, with the exception of Figure 39 (see p. 38). References and data sources are listed at the end of the report.

Air temperatures

Air temperatures measured near the planet's surface (surface air temperatures) are at the centre of many climate discussions, but the significance of any short-term warming or cooling should not be overstated. Whenever the Earth experiences warm El Niño or cold La Niña episodes, major heat exchanges take place between the Pacific Ocean and the atmosphere above, eventually showing up as a signal in the global air temperature. However, such heat exchanges may chiefly reflect redistribution of energy between ocean and atmosphere, and not a change in the heat content of the atmosphere–ocean system. Evaluating the dynamics of ocean temperatures is therefore just as important as evaluating changes in surface air temperatures.

Considering surface air temperature records since the 19th century, 2021 was a warm year, but cooler than most years since 2016. A moderate La Niña episode played out during 2021, underlining the importance of ocean–atmosphere exchanges.

Many Arctic regions experienced record high air temperatures in 2016, but since then, including in 2021, conditions have generally moved toward somewhat cooler conditions. The temperature peak in high northern latitudes in 2016 may have been affected by ocean heat released from the Pacific Ocean during the strong 2015–16 El Niño and subsequently transported towards the Arctic region. This underscores how air temperatures may be affected, not only by variations in local conditions, but also by variations playing out in geographically remote regions.

Many figures in this report focus on the period since 1979 – the satellite era – when access to a wide range of observations with nearly global coverage, including temperature, became commonplace. These data provide a detailed view into temperature changes over time at different altitudes in the atmosphere. Among other phenomena, these observations reveal that a Stratospheric temperature plateau has prevailed since 1995.

Since 1979, lower Troposphere temperatures have increased over both land and oceans, but most clearly over the land. The most straightforward explanation for this is that much of the warming is caused by solar insolation, but there may be several secondary reasons, such as changes in cloud cover and land use.

Oceans

The Argo Program, which uses robotic floats to monitor ocean temperatures around the globe, and at different depths, has now achieved 18 years of global coverage, growing from a relatively sparse array of 1000 floats in 2004 to more than 3900 in December 2021. Since 2004, these floats have provided a unique ocean temperature dataset for depths down to 1900 m. The data is currently updated to August 2020.

Although the oceans are much deeper than 1900 m, and the published Argo data series still is relatively short, interesting features are now emerging from these observations. For example, since 2004, the upper 1900 m of the oceans have experienced a globally averaged net warming of about 0.07°C. The maximum net warming (about 0.2°C) affects the uppermost 100 m, mainly near the Equator, where the greatest amount of solar radiation is received. At greater depths, a small (about 0.025°C) net warming has occurred between 2004 and 2020, according to the Argo floats. Warming is seen across the Equatorial oceans, which, due to the spherical form of the planet, represent a huge surface area.

Simultaneously, the northern oceans (55–65°N) have experienced a marked cooling at depths down to 1400 m, and slight warming below that. The southern oceans (55–65°S) have warmed slightly at most depths since 2004, but mainly near the surface. However, as discussed later in this report, averages may be misleading, and better insight is often gained by looking at the details.

Sea level

Global sea level is monitored by satellite altimetry and by direct measurement using tide gauges. While the satellite record suggests a global sea-level rise of about 3.3 mm per year or more, data from tide gauges all over the world suggest a stable rise of 1–2 mm per year. The tide gauges indicate no recent acceleration (or deceleration) of sea-level rise. The marked difference (a ratio of about 1:2) between the two datasets has no universally accepted explanation, but it is known that the satellite observations face complications in areas near the coast (see, for example, Vignudelli et al. 2019). Whatever the truth, the tide-gauge data are more relevant for local coastal planning purposes.

Sea ice

In 2021, global sea-ice cover remained well below the average for the satellite era, but is now increasing. At the end of 2016, it reached a marked minimum, at least partly caused by the operation of two different natural variation patterns, affecting sea ice in the Northern and the Southern Hemisphere, respectively. These variations had simultaneous minima in 2016. The trend towards stable or higher ice extent at both poles probably began in 2018, and has since strengthened. The marked Antarctic 2016 sea-ice reduction was the result of unusual wind conditions.

Snow cover

Variations in global snow cover are mainly caused by changes in the Northern Hemisphere, where all the major land areas are located. Southern Hemisphere snow is mainly found in the Antarctic, and cover is therefore relatively stable. The Northern Hemisphere average snow cover has been stable since the onset of satellite observations, although local and regional interannual variations may be large. Since 1979, Northern Hemisphere snow cover in autumn has been slightly increasing, the mid-winter cover is basically stable, and the spring cover is slightly decreasing. In 2021, the Northern Hemisphere seasonal snow cover was close to the 1972–2020 average.

Storms and hurricanes

The most recent data on global tropical storm and hurricane accumulated cyclone energy (ACE) is well within the range observed since 1970. In fact, the ACE data is highly variable over time, with a significant 3.6-year variation, but without any clear trend towards higher or lower values. A longer series for the Atlantic Basin, however, indicates there may be an oscillation of about 60 years' duration for tropical storm and hurricane ACE. The number of hurricanes making landfall in the continental United States remains within the range for the entire observation period since 1851.

1. Air temperatures

Surface: spatial pattern

The year 2021 was affected by a cold La Niña episode (see below for detailed discussion). Global average surface air temperatures were lower than in recent years, and it looks as if 2016 may have been a global temperature peak. The next few years will show if this suggestion is correct.

The Northern Hemisphere was characterised by regional temperature contrasts, especially north of 30°N. The most pronounced temperature event in 2021 was the development of low average temperatures (compared to the last 10 years) in Russia and Siberia, in strong contrast to the warm conditions in these regions in 2020. These regions, together with Alaska, encompass some of the largest permafrost regions on Earth.

Near the Equator, surface air temperatures were generally near or below the average for the previous 10 years. In the Pacific Ocean, cooler conditions reflected the ongoing La Niña episode.

In the Southern Hemisphere, surface air temperatures were near or below the average for the previous 10 years. Australia, in particular, was cool.

In the Arctic, the Europe-Russia-Siberia-Alaska sectors were relatively cold, while most of the Canada-Greenland sectors were relatively warm.

The Antarctic saw temperatures near or below the 10-year average.

In summary, global average air temperatures in 2021 were still high when framed against the full instrumental period (since 1850/1880), but exhibit a negative trend since 2016. The influence of a La Niña episode in the Pacific Ocean shows that the global surface air temperature record continues to be highly influenced by oceanographic phenomena.

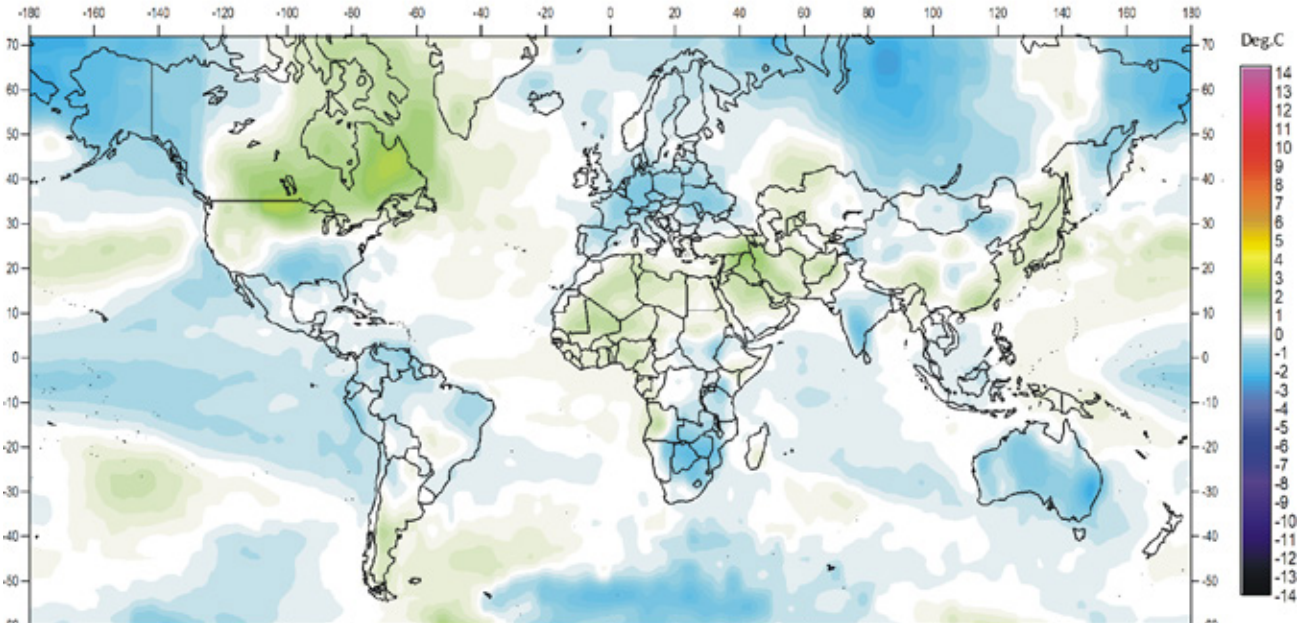

Figure 1: 2021 surface air temperatures compared to the average for the previous 10 years.

Green-yellow-red colours indicate areas with higher temperature than the average, while blue colours indicate lower than average temperatures. Data source: Remote Sensed Surface Temperature Anomaly, AIRS/Aqua L3 Monthly Standard Physical Retrieval 1-degree x 1-degree V007 (https://airs.jpl.nasa.gov/), obtained from the GISS data portal (https://data.giss.nasa.gov/gistemp/maps/index_v4.html).

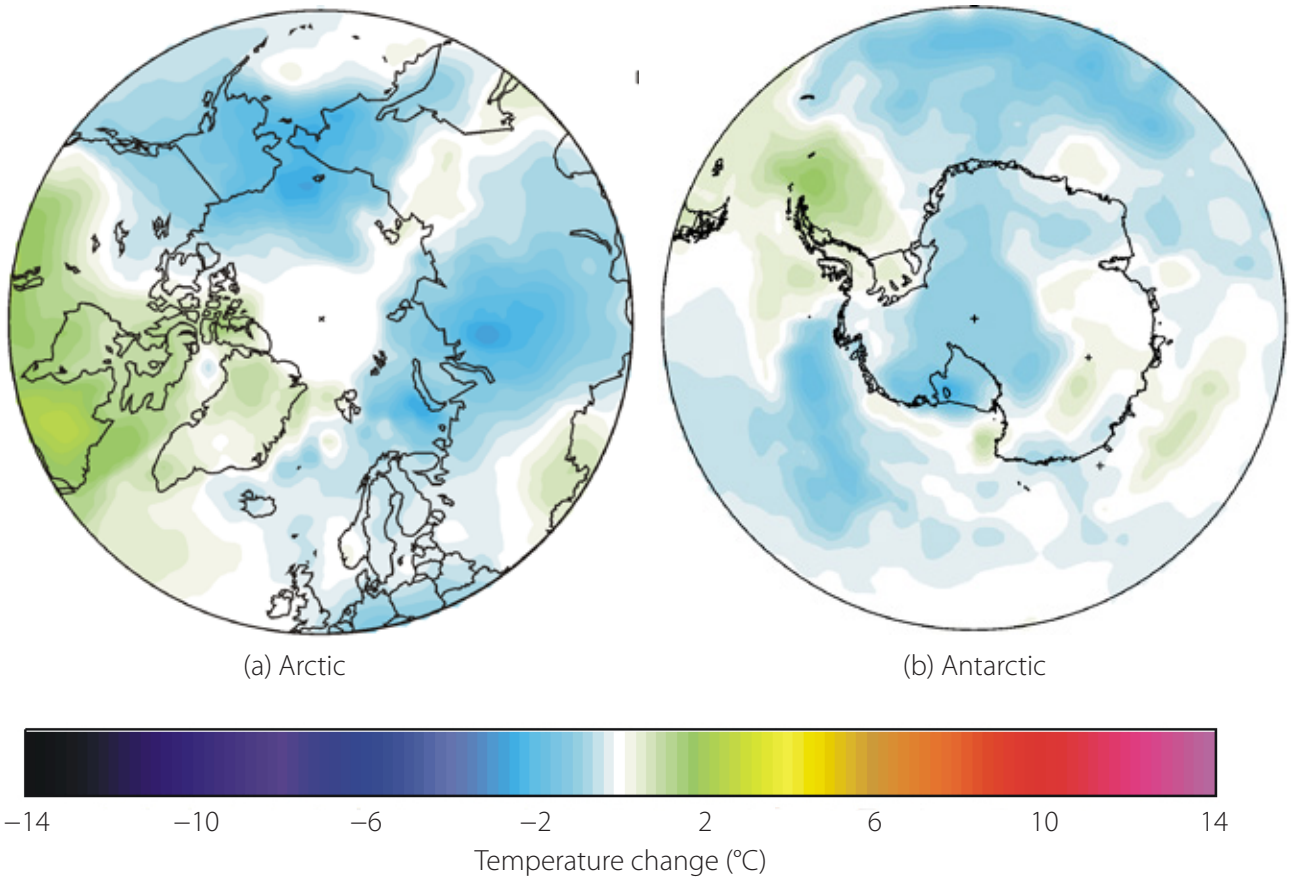

Figure 2: 2021 polar surface air temperatures compared to the average for the previous 10 years.

Green-yellow-red colours indicate areas with higher temperature than the average, while blue colours indicate lower than average temperatures. Data source: Remote Sensed Surface Temperature Anomaly, AIRS/Aqua L3 Monthly Standard Physical Retrieval 1-degree × 1-degree V007 (https://airs.jpl.nasa.gov/), obtained from the GISS data portal (https://data.giss.nasa.gov/gistemp/maps/index_v4.html).

Lower Troposphere: monthly

Both satellite records for the lower Troposphere temperature clearly show a temperature spike associated with the 2015–16 El Niño, a subsequent gradual drop, followed by a new temperature spike due to the moderate 2019–20 El Niño. The latest development is a renewed temperature drop.

The overall temperature variation in the diagrams (Figures 3–4) is similar for the two data series, but the overall temperature rise over the period 1979–2021 is larger for RSS than for UAH. Before the rather marked adjustment of the RSS series in 2017, the temperature increase was almost identical for the two data series.

(a) UAH

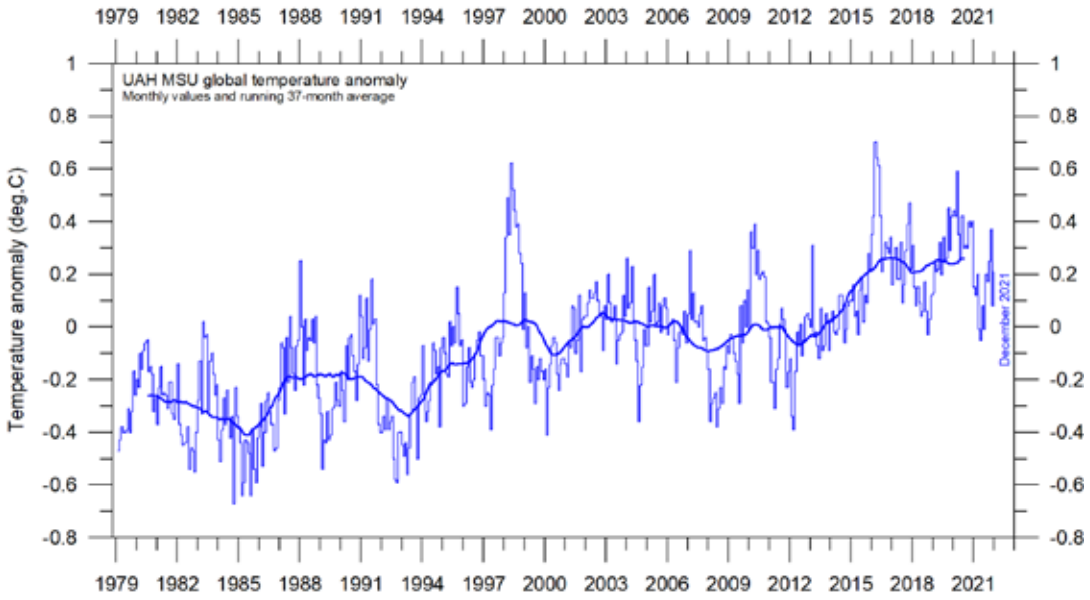

(b) RSS

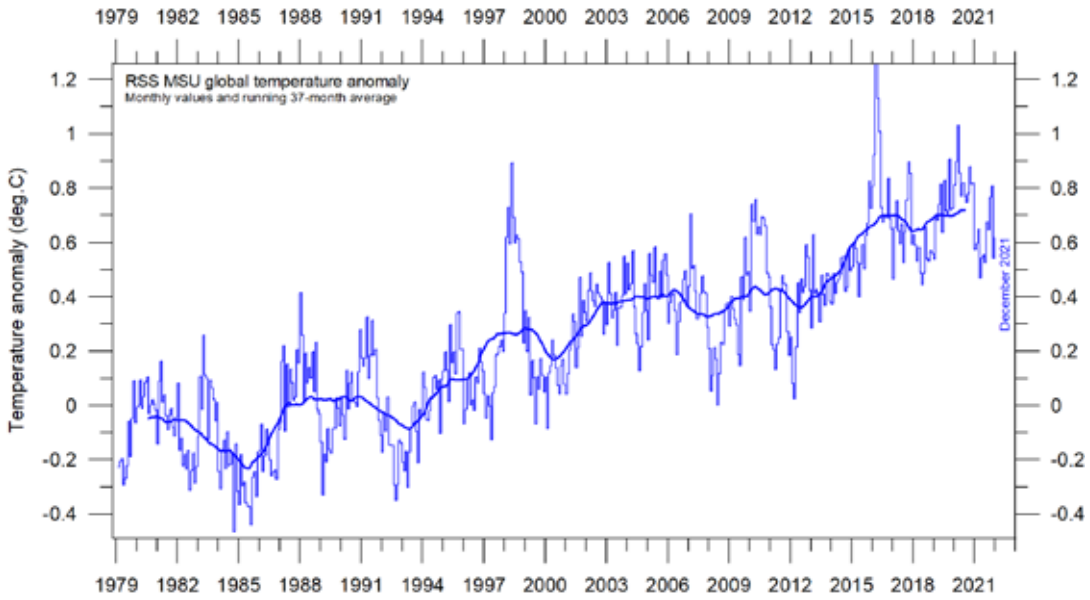

Figure 3: Global monthly average lower troposphere temperatures since 1979.

(a) UAH and (b) RSS. The thick line is the simple running 37-month average, nearly corresponding to a running 3-year average.

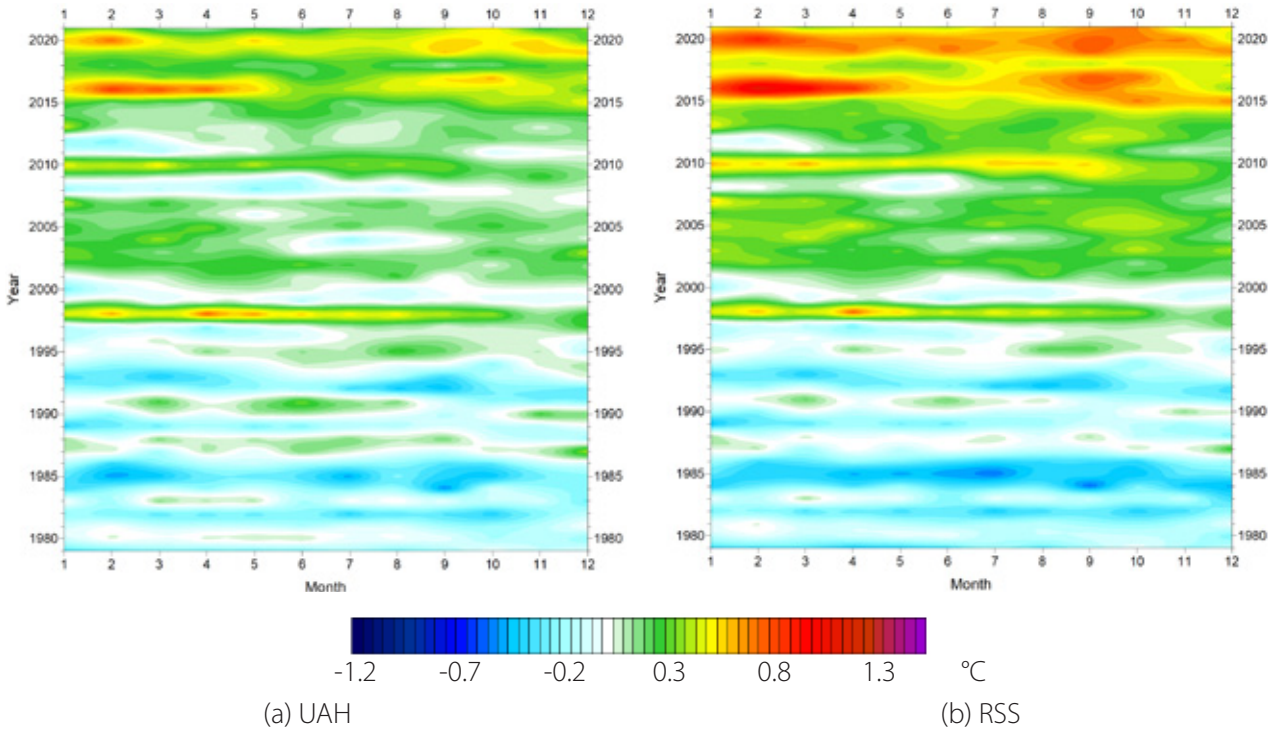

Figure 4: Temporal evolution of global lower troposphere temperatures since 1979.

Temperature anomaly versus 1979–2008. The effects of the El Niños of 1998, 2010 and 2015–2016 are clearly visible, as are the tendency for many El Niños to culminate during the Northern Hemisphere winter. As the different temperature databases are using different reference periods, the series have been made comparable by setting their individual 30-year average (1979–2008) to zero.

Lower Troposphere: annual means

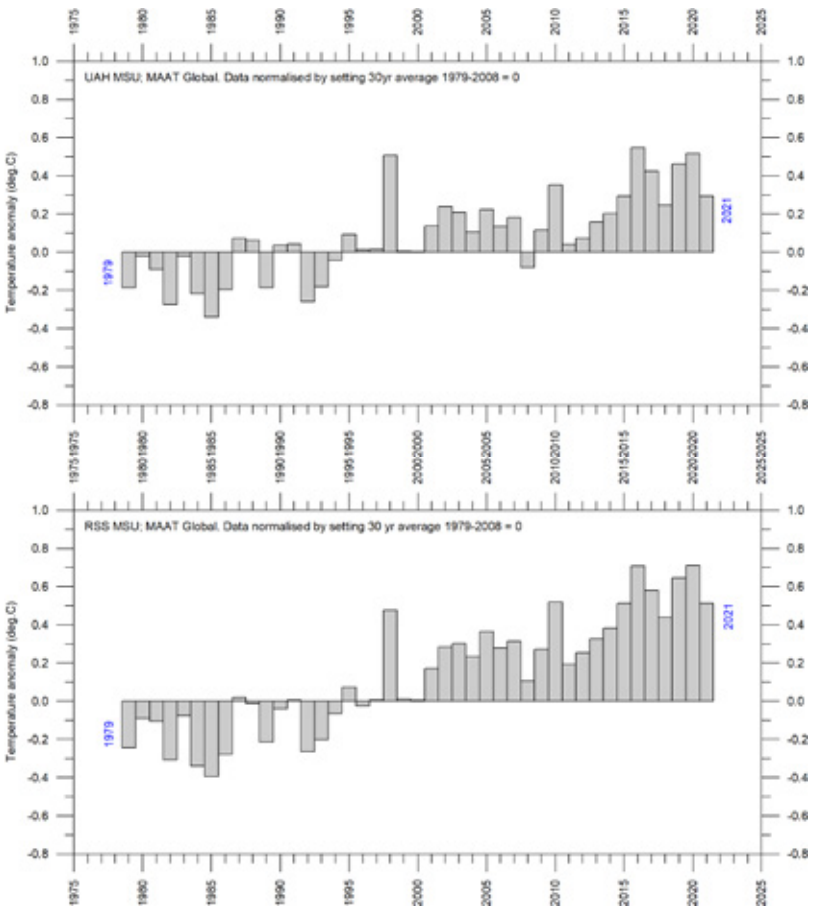

Figure 5: Global mean annual lower troposphere air temperatures since 1979.

Satellite data interpreted by the University of Alabama at Huntsville (UAH), and Remote Sensing Systems (RSS), both in the USA.

Surface: monthly

All three surface air temperature records clearly show the temperature spike associated with the 2015–16 El Niño, the subsequent temperature drop, and the renewed temperature increase due to the moderate 2019–20 El Niño (Figure 6).

They also, however, confirm that the recent major El Niño episode culminated in early 2016, and was followed by a gradual return towards pre-2015 conditions, a renewed increase in 2019 and then the latest temperature decrease. This development is also shown in Figures 6–7.

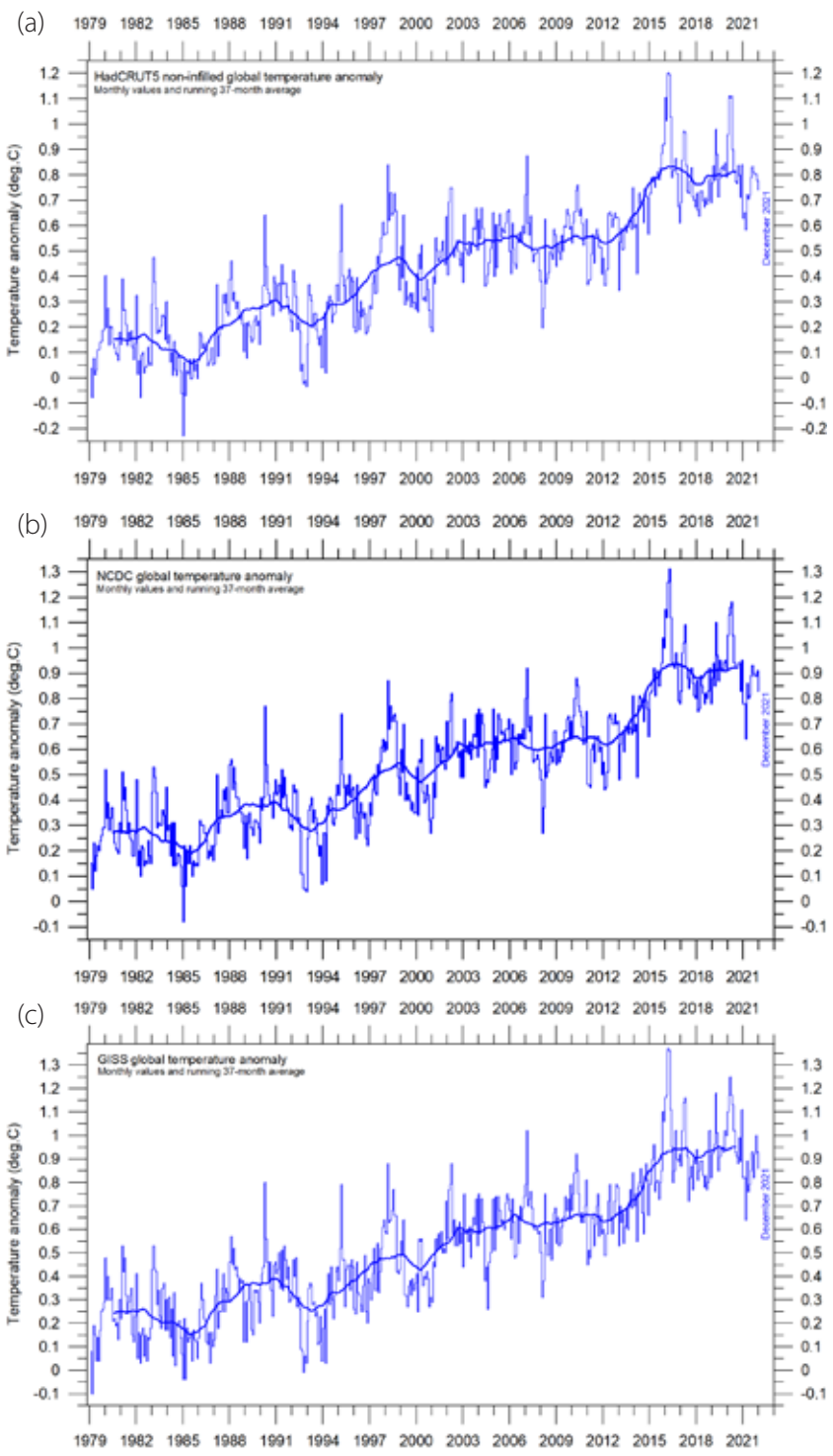

Figure 6: Global mean monthly surface air temperatures since 1979.

(a) HadCRUT4 (b) NCDC (c) GISS. The thick line is the simple running 37-month average, nearly corresponding to a running 3-year average.

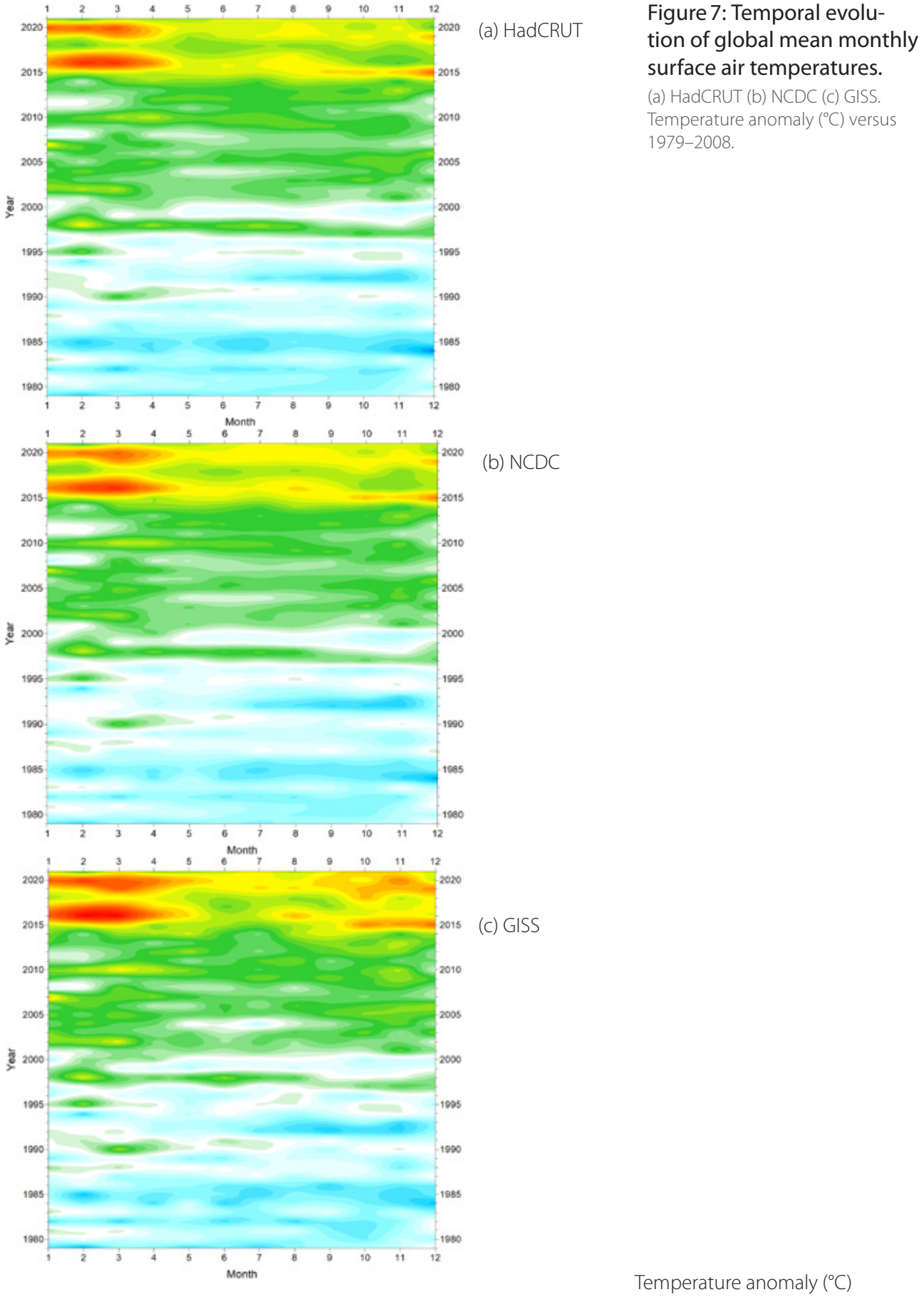

Figure 7: Temporal evolution of global mean monthly surface air temperatures.

(a) HadCRUT (b) NCDC (c) GISS. Temperature anomaly (°C) versus 1979–2008.

Surface: annual means

All three average surface air temperature estimates show the year 2021 to be cooler than most years since 2016 (Figure 8). As noted already, 2021 was influenced by a La Niña episode playing out in the Pacific Ocean (see Figure 23).

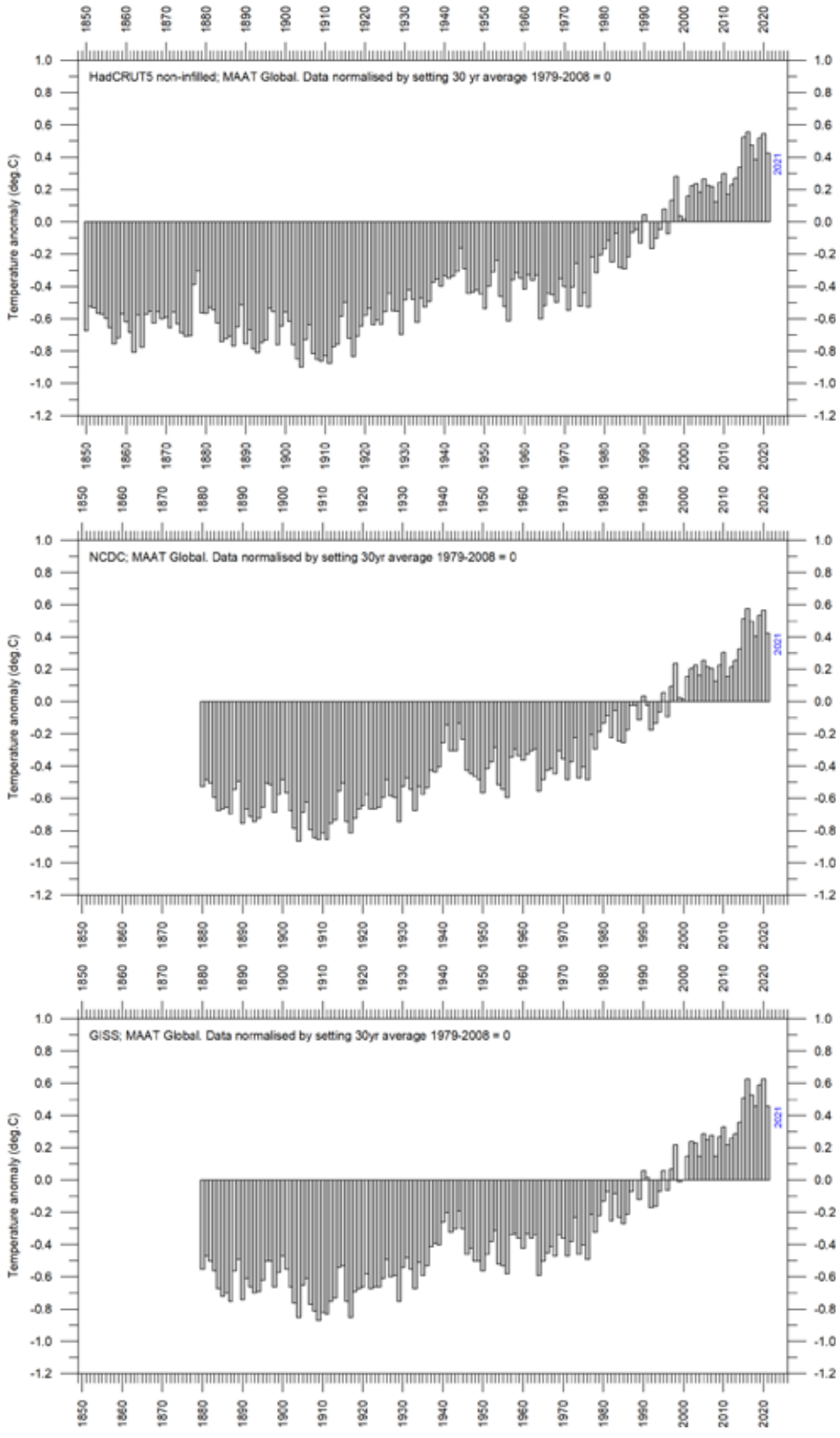

Figure 8: Global mean annual surface air temperatures.

(a) HadCRUT (b) NCDC (c) GISS. temperature anomaly (°C) versus 1979–2008.

Error, consistency and quality

Air temperatures in 2021 were high relative to the full lengths of the various records (since 1850, 1880, or, for the satellites, 1979). The surface records represent a blend of sea surface data collected by moving ships or by other means, plus data from land stations, of partly unknown quality and unknown degree of representativeness for their region. Moreover, many of the land stations have moved geographically during their period of operation, instrumentation has been changed, and most are influenced by ongoing changes in their surroundings (vegetation, buildings, and so on).

The satellite temperature records have their own problems, but these are generally of a more technical nature and are therefore more readily correctable. In addition, the temperature sampling by satellites is more regular and complete on a global basis than that in the surface records. It is also important to note that the sensors on satellites measure temperature directly (by emitted radiation), while most modern surface temperature measurements are indirect, using electronic resistance.

All temperature records are affected by at least three sources of error, each of which differs among the individual station records used.

- The *accuracy* is the degree of closeness of measurements to the actual (true) values.
- The *precision* is the degree to which repeated measurements under unchanged conditions show an identical value, true or not.
- The *measurement resolution* is the smallest change in temperature that produces a response in the instrument used for measurement.

When combined, these give the margin of error for the record. The margin of error has been thoroughly discussed by scientists, and is probably at least ±0.1°C for surface air temperature records. This often makes it statistically impossible to classify any year as 'record-breaking', as several other years may be within the margin of error.

In addition, two other issues relating to the margin of error for surface records have not received so much attention. First, as an example, it will not be possible to conclude much about the actual value of the December 2021 global surface air temperature before March or April 2022, when remaining measurements are finally incorporated in the surface air temperature databases. This is what might be described as the effect of delayed reporting. Secondly, the surface air temperature records often display administrative changes over time, which makes it even more difficult to conclude anything about the significance of recently reported monthly or annual surface air temperatures.

The administrative issue arises from the apparently perpetual retrospective changes to the values recorded in the temperature databases, with the consequence that what was reported as the average global temperature for one year will later change. This has little or nothing to do with delayed reporting: in all of the datasets (but particularly GISS and NCDC), changes are still being made to years in the distant past, even in the 19th century, where the likelihood of delayed data reporting is exceedingly small. Most likely, it is the result of alterations to the way average monthly values are calculated, in an attempt to enhance the resulting record.

As an example of the effect, Figure 9 shows the accumulated effect since May 2008 of such administrative changes in the GISS global surface air temperature record, extending back to 1880. The overall net effect is warming of the early and modern part of the record and cooling of the period in between, roughly from 1900 to 1970. The changes in annual values are sometimes quite substantial, ranging from about +0.15 to −0.15°C.

To illustrate the effect of administrative changes in a different way, Figure 10 shows how the global surface air temperatures for January 1910 and January 2000 (months indicated in Figure 15) have changed since May 2008, again exemplified by the GISS record.

The temperature difference between January 1915 and January 2000 has increased from 0.45°C (as reported in May 2008) to 0.67°C (as reported in January 2022). This represents an increase of about 49% over this period, mean-

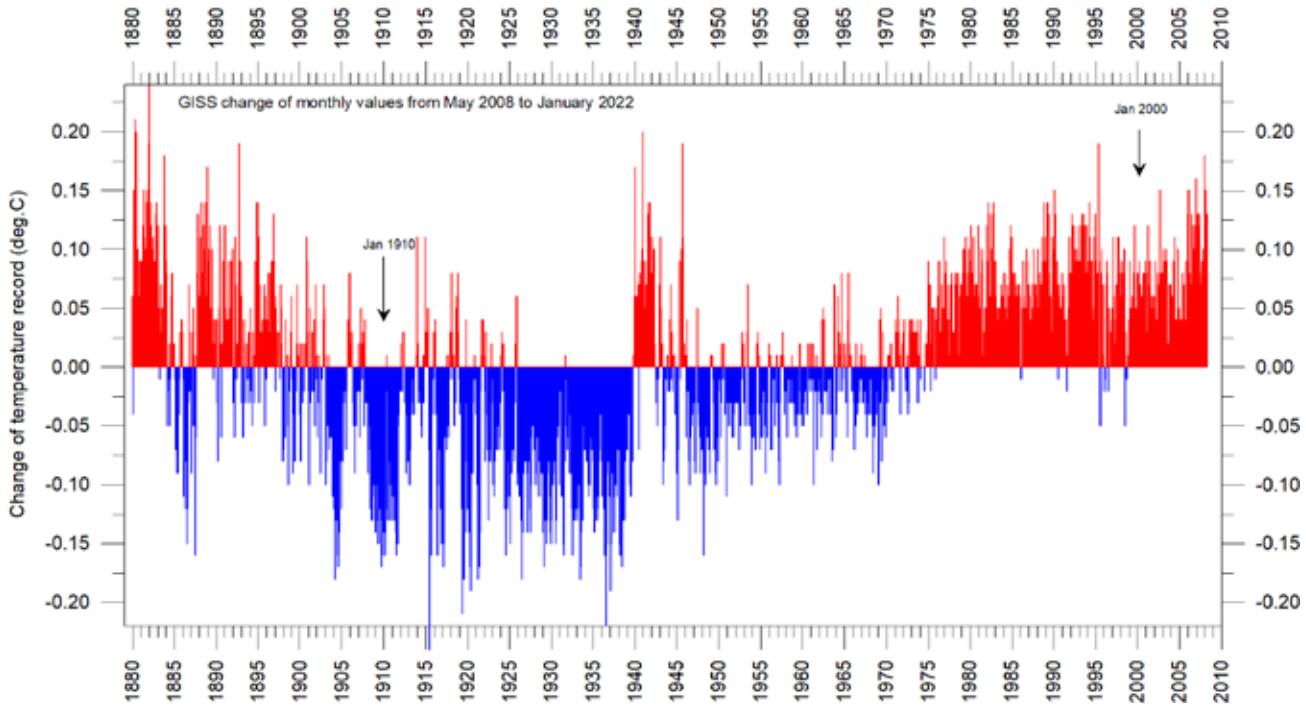

Figure 9: Adjustments since 17 May 2008 in the GISS surface temperature record.

ing that about half of the apparent global temperature increase from January 1910 to January 2000 is due to administrative adjustments to the original data made since May 2008. Clearly such alterations are important when evaluating the overall quality of various temperature records, along with other standard sources of error. In fact, the magnitude of administrative changes may exceed the formal margin of error.

In 2021, a new version of the HadCRUT database was introduced. HadCRUT5 comes in two sub-versions, known as HadCRUT5analysis and HadCRUT5non-infilled, respectively. Both provide global historical surface temperature anomalies relative to a 1961–1990 reference period. As with the previous version, HadCRUT4, in HadCRUT5 data are averaged onto a regular grid, with no value provided in grid cells containing no observations. For HadCRUT5analysis, a statistical method has subsequently been used to model coverage in grid cells without observations, to provide a more globally complete data set. For HadCRUT5non-infilled, this is not the case (as with HadCRUT4). Figure 11 below shows the differences between HadCRUT4, HadCRUT5non-infilled and HadCRUT5analysis.

The overall effect of the version change from HadCRUT4 to HadCRUT5 is an apparent cooling of the time period 1880–1975, and an apparent warming before 1880 and after 1975. The apparent warming and cooling are about +0.1 and −0.1°C, respectively (Figure 11). The version change conveys the impression of a somewhat more rapid global temperature increase following the relatively cold period terminating around 1975. In the present report, data from the HadCRUT5non-infilled version is used, so as to keep the focus on observations.

Everybody interested in climate science should acknowledge the efforts put into maintaining the different temperature databases referred to in the present report. At the same time, however, it is also important to realise that all temperature records cannot be of equal scientific quality. The simple fact that they to some degree differ shows that they cannot all be completely correct.

Figure 10: Adjustments made since May 2008 to GISS anomalies for the months January 1910 and January 2000.

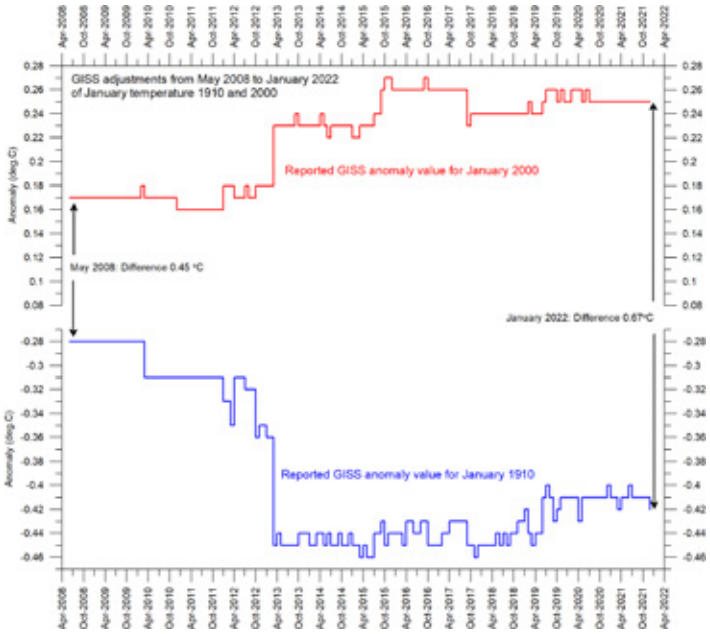

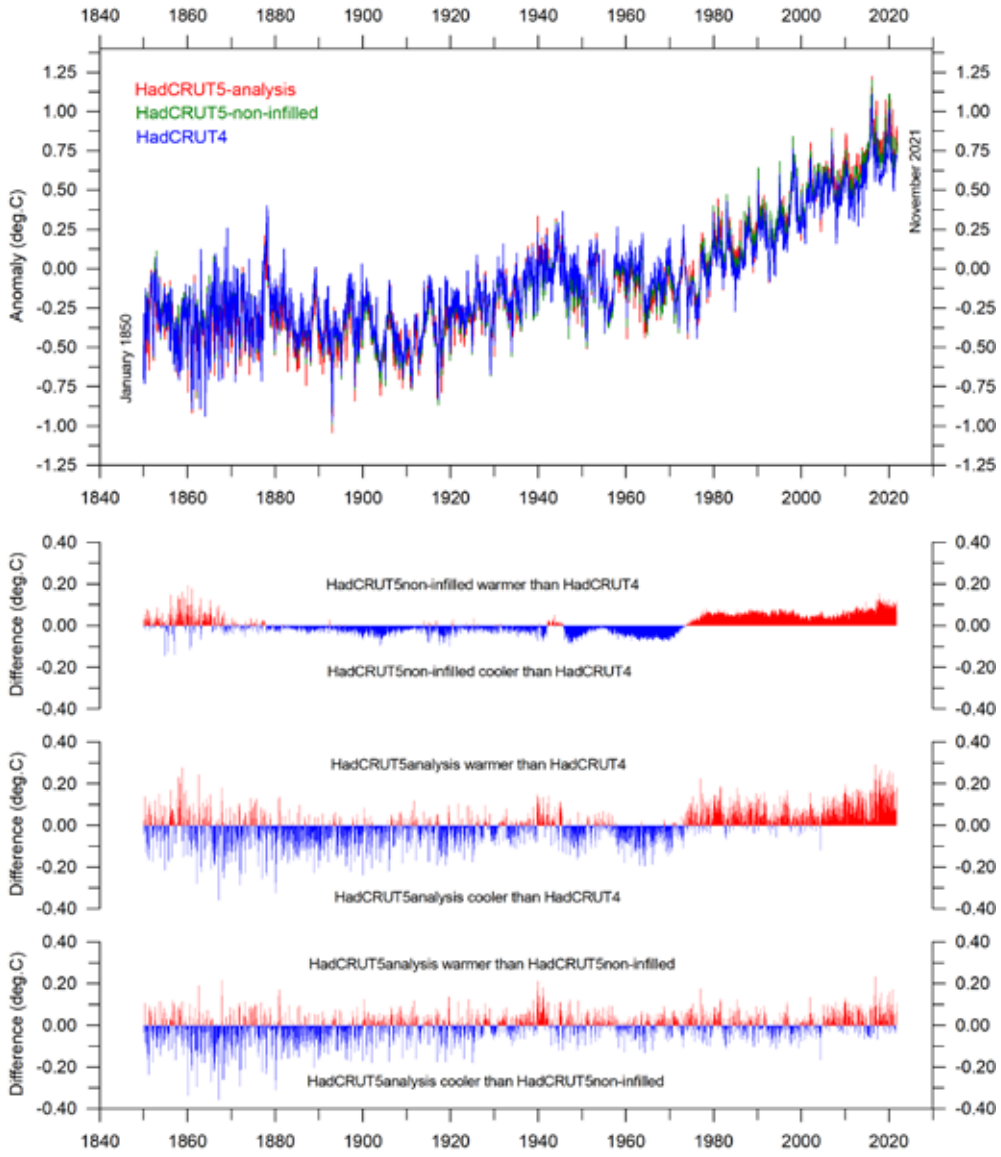

Figure 11: Differences between HadCRUT4, HadCRUT5non-infilled and HadCRUT5analysis.

Surface versus lower Troposphere

In general, there is fair agreement between the average of surface- and satellite records, as shown in Figure 12. However, before the major adjustment of the RSS satellite record in 2017, the situation was different, with the average of surface records drifting in a warmer direction than the average of the satellite records. Again, this illustrates the importance of ongoing changes made to the individual temperature records.

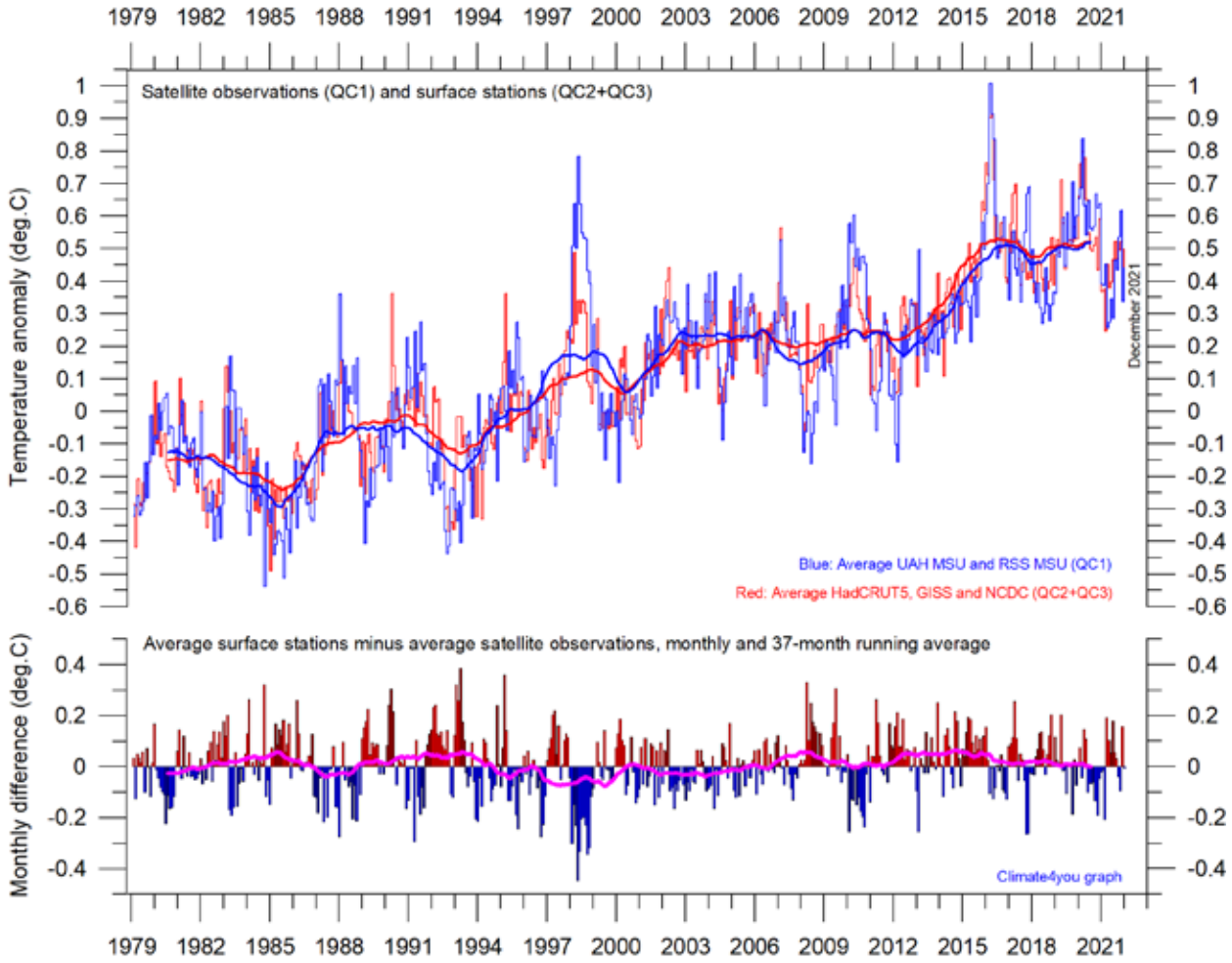

Figure 12: Surface temperatures versus lower Troposphere temperatures.

Average of monthly global surface air temperature estimates (HadCRUT, NCDC and GISS) and satellite-based lower Troposphere temperature estimates (UAH and RSS). The thin lines indicate the monthly value, while the thick lines represent the simple running 37-month average, nearly corresponding to a running 3-year average. The lower panel shows the monthly difference between surface air temperature and satellite temperatures. As the base period differs for the different temperature estimates, they have all been normalised by comparing to the average value of 30 years from January 1979 to December 2008.

Lower Troposphere: land versus ocean

Since 1979, the lower Troposphere has warmed considerably more over land than over the oceans. There may be several reasons for this, such as variations in incoming solar radiation, cloud cover and land use.

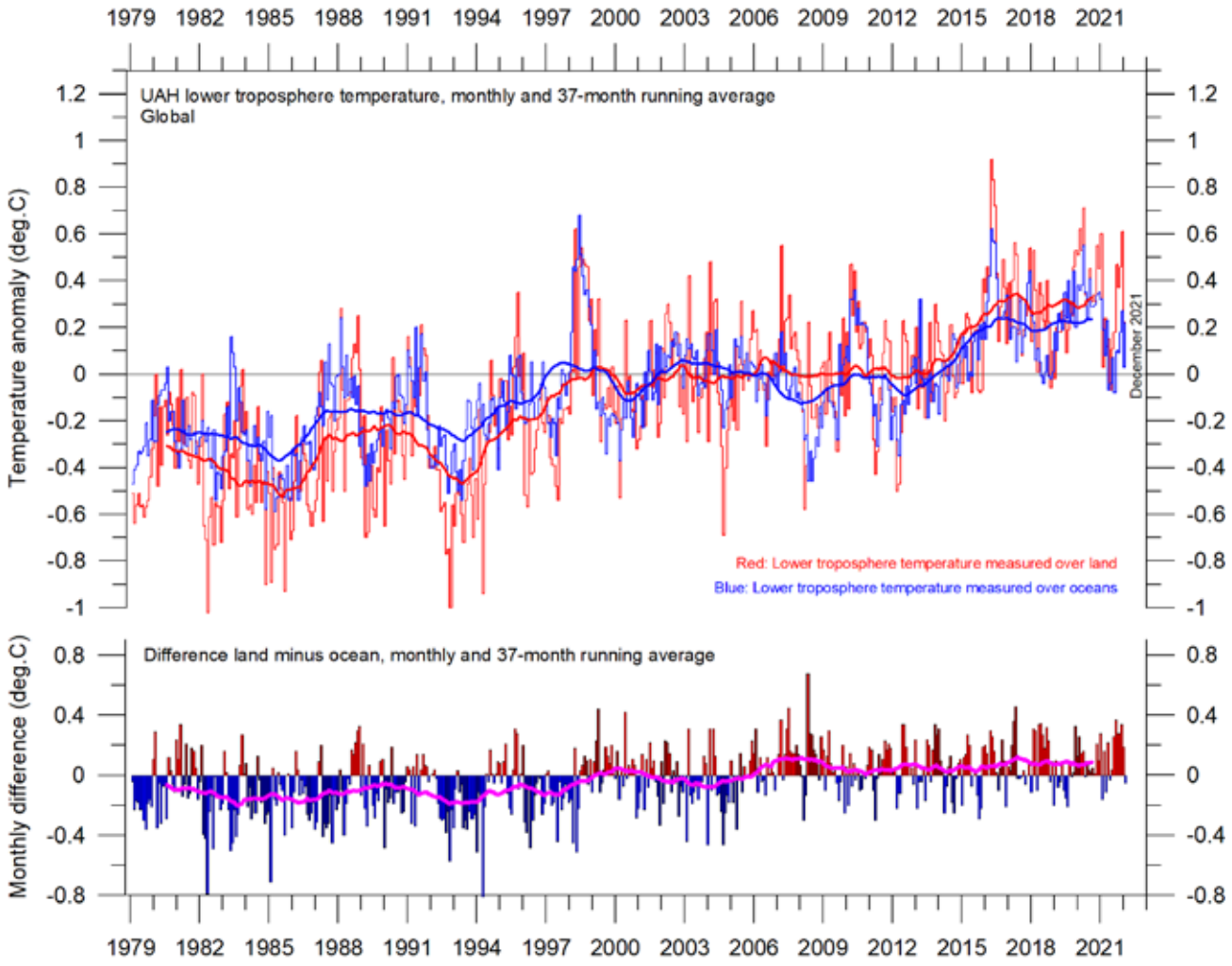

Figure 13: Lower Troposphere temperatures over land and ocean

Global monthly average lower troposphere temperature since 1979 measured over land and oceans, shown in red and blue, respectively, according to University of Alabama at Huntsville (UAH), USA. The thin lines represent the monthly average, and the thick line the simple running 37-month average, nearly corresponding to a running 3-year average.

By altitude

Changes in the vertical temperature profile of the atmosphere are interesting for several reasons. One reason is that increasing Tropospheric temperatures and decreasing Stratospheric temperatures are two central features of the hypothesis ascribing global warming to anthropogenic increases in atmospheric carbon dioxide.

The temperature variations recorded in the lowermost Troposphere are generally reflected at higher altitudes, up to about 10 km, including many individual lows and peaks, such as the El Niño induced temperature peak of 2015–16.

At high altitudes, near the Tropopause, the pattern of variations recorded lower in the atmosphere can still be recognised, but for the duration of the record (since 1979) there has been no clear trend towards higher or lower temperatures.

Higher in the atmosphere, in the Stratosphere, at 17 km altitude, two pronounced temperature spikes are visible before the turn of the century. Both can be related to major volcanic eruptions, as indicated in the figure. Ignoring these spikes, until about 1995 there is a persistent and marked temperature decline, ascribed by some scientists to the effect of heat being

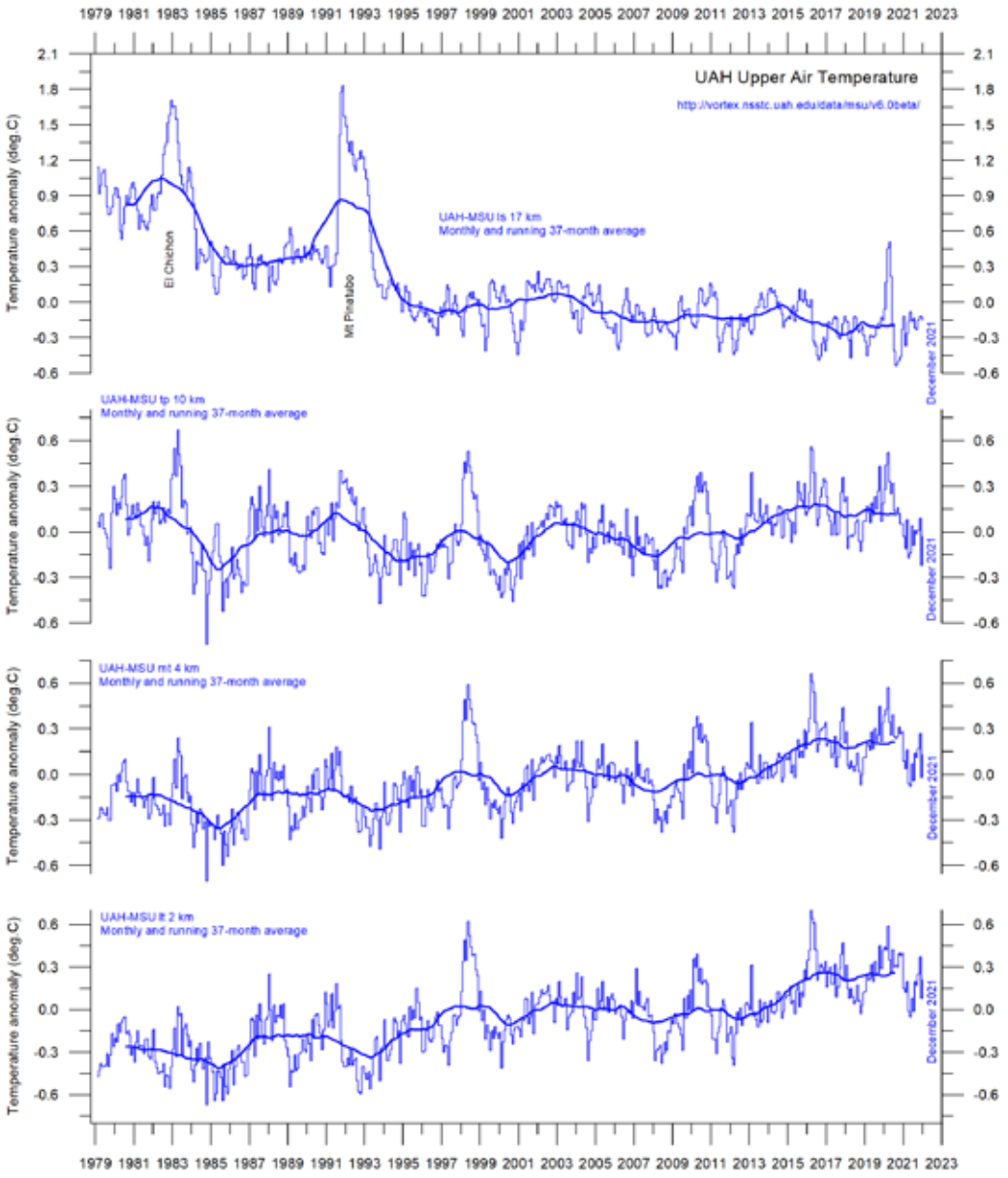

Figure 14: Temperature by altitude.

Global monthly average temperature in different altitudes according to University of Alabama at Huntsville (UAH), USA. The thin lines represent the monthly average, and the thick line the simple running 37-month average, nearly corresponding to a running 3-year average.

trapped by carbon dioxide in the Troposphere below. However, the marked declined in temperatures essentially ended around 1995–96, since when there has been a long temperature plateau. In 2020, however, there was a marked, but short-lived, temperature peak, rapidly followed by an equal drop in temperature. Since the end of 2020, temperatures have been back at the pre-2020 level.

Zonal air temperatures

Figure 15 shows that the 'global' warming experienced since 1980 has predominantly been a Northern Hemisphere phenomenon, and mainly played out as a step change between 1994 and 1999. This rapid temperature change was, however, influenced by the Mt. Pinatubo eruption 1992–93 and the later 1997 El Niño episode.

Figure 15 also reveals how the temperature effects of the strong El Niños in 1997 and 2015–16, as well as the moderate one in 2019, apparently spread to higher latitudes in both hemispheres after a delay. This El Niño temperature effect was, however, mainly recorded in the Northern Hemisphere, and only to lesser degree in the Southern Hemisphere.

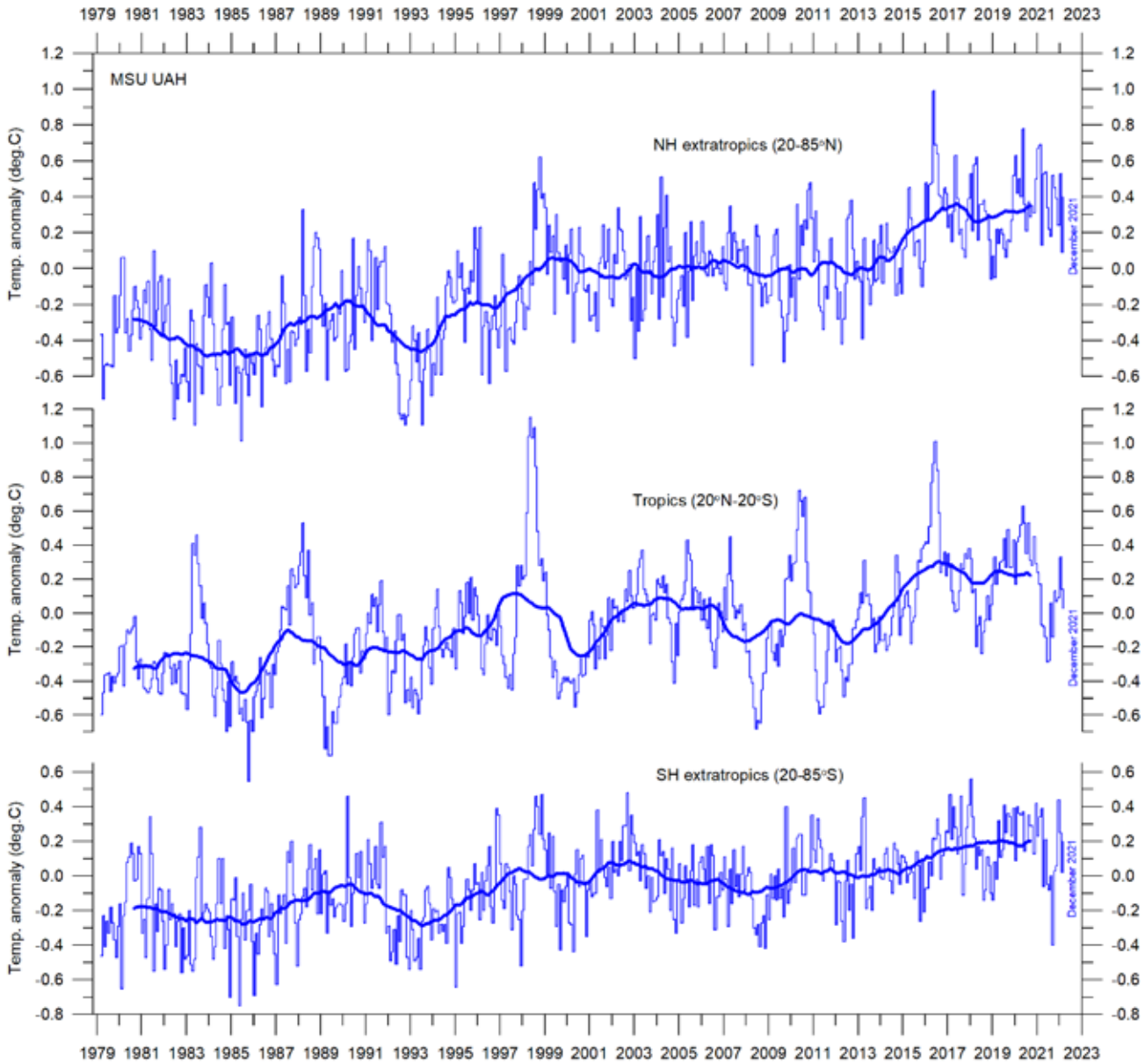

Figure 15: Zonal air temperatures

Global monthly average lower troposphere temperature since 1979 for the tropics and the northern and southern extratropics, according to University of Alabama at Huntsville, USA. Thin lines: monthly value; thick lines: 3-year running mean.

Polar air temperatures

In the Arctic, warming mainly took place in the period 1994–96, and less so subsequently (Figure 16). In 2016, however, temperatures peaked for several months, presumably because of oceanic heat given off to the atmosphere during the El Niño of 2015–16 (see also Figure 23) and then advected to higher latitudes. A slight temperature decrease has characterised the Arctic since 2016.

In the Antarctic region, temperatures have remained almost stable since the onset of the satellite record in 1979. In 2016–17, a small temperature peak visible in the monthly record may be interpreted as the attenuated effect of the recent El Niño episode.

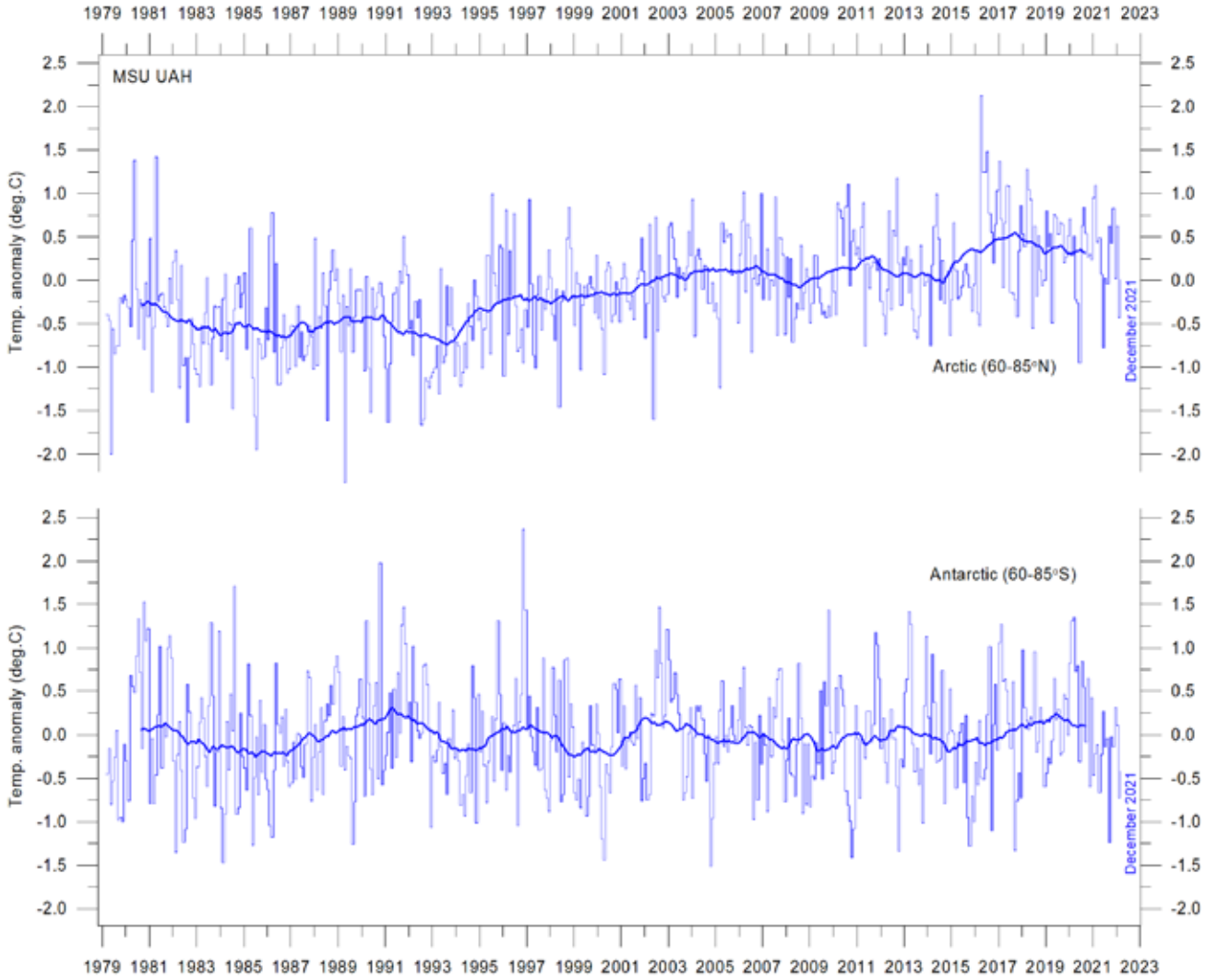

Figure 16: Polar temperatures

Global monthly average lower troposphere temperature since 1979 for the North Pole and South Pole regions, according to University of Alabama at Huntsville, USA. Thick lines are the simple running 37-month average.

2. Atmospheric greenhouse gases

Water vapour

Water vapour is the most important greenhouse gas in the Troposphere. The highest concentration is found in a latitudinal range from 50°N to 60°S. The two polar regions of the Troposphere are comparatively dry. Water vapour is a much more important greenhouse gas than carbon dioxide, both in terms of its absorption spectrum and its concentration in the atmosphere.

Figure 17 shows the specific atmospheric humidity to be stable or slightly increasing up to about 4–5 km altitude. At higher levels in the Troposphere (about 9 km), the specific humidity has been decreasing for the duration of the record (since 1948), but with shorter variations superimposed on the falling trend. A Fourier frequency analysis (not shown here) shows these changes to be influenced not only by annual variations, but also by a periodic variation of about 34.5 years' duration.

The slight, but persistent, decrease in specific humidity at about 9 km altitude is remarkable, as this altitude roughly corresponds to the level where the theoretical temperature effect of increased atmospheric carbon dioxide is expected to play out initially.

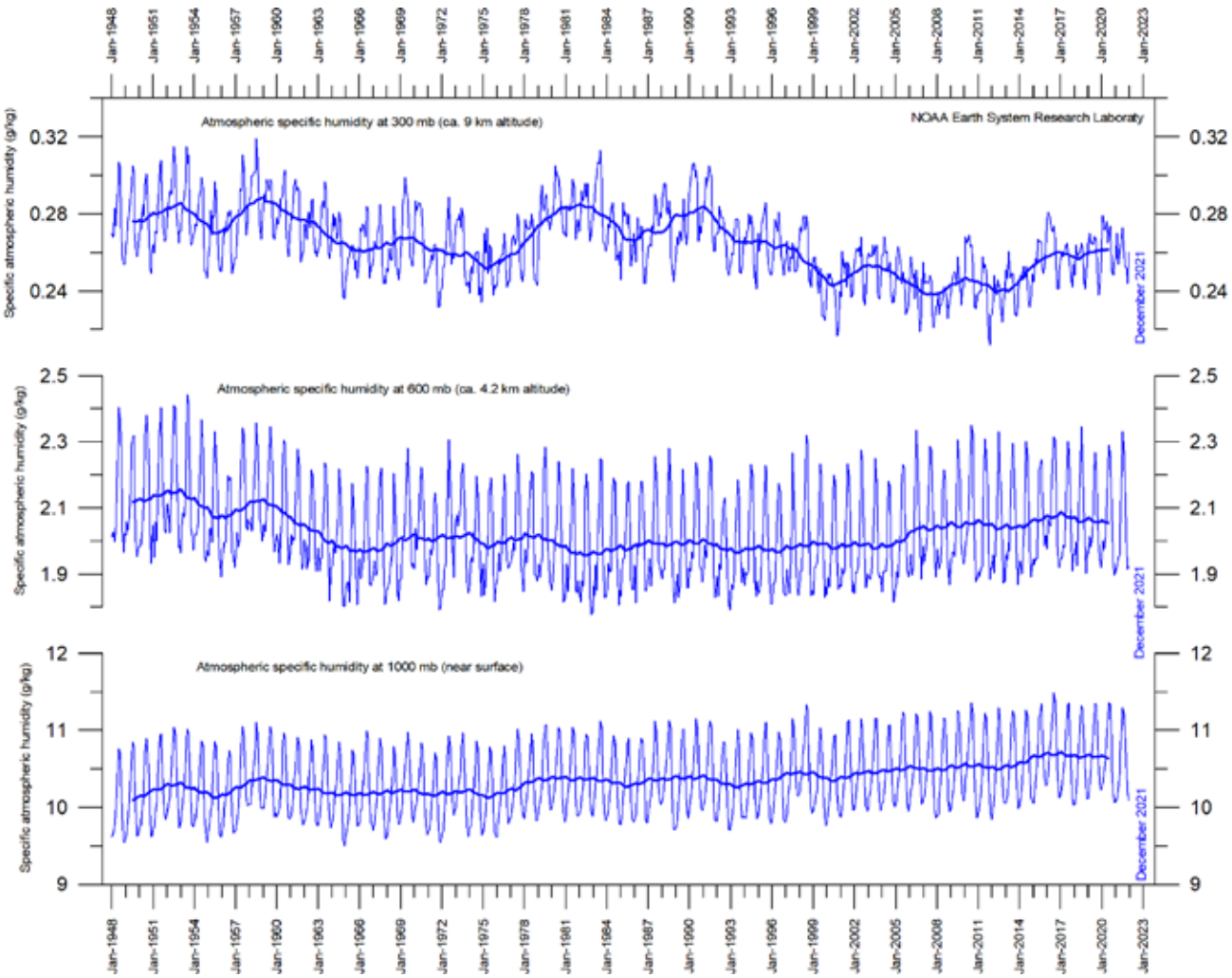

Figure 17: Humidity.

Specific atmospheric humidity (g/kg) at three different altitudes in the Troposphere since January 1948. The thin blue lines show monthly values, while the thick blue lines show the running 37-month average (about 3 years). Data source: Earth System Research Laboratory (NOAA).

Carbon dioxide

Carbon dioxide is an important greenhouse gas, although less important than water vapour. Concentrations have been increasing for the duration of the Mauna Loa record (since 1958), although with an annual cycle superimposed on the trend (Figure 18). At the end of 2021, the atmospheric concentration was close to 417 parts per million (ppm).

Carbon dioxide is usually considered a relatively well-mixed gas in the Troposphere. The annual change in Tropospheric concentration has been increasing, from about +1 ppm/year in the early part of the record to about +2.6 ppm/year towards the end of the record (Figure 19). A Fourier frequency analysis (not shown here) suggests the annual change of Tropospheric carbon dioxide is influenced by a significant periodic variation of 3.6-years' duration. Since January 2020, there has been no visible effect of the global COVID-19 lockdown on atmospheric concentrations.

It is informative to examine the annual change in atmospheric CO_2 alongside the annual changes in global air temperature and global sea-surface temperature (Figure 20). All three vary in concert, but with sea-surface temperatures leading a few months ahead of the global temperature and change rates for atmospheric CO_2 lagging 11–12 months behind the sea-surface temperature change rates. Important changes apparently originate at the sea surface.

Figure 21 shows the visual association between annual change of atmospheric CO_2 and La Niña and El Niño episodes, emphasising the importance of oceanographic dynamics for understanding changes in atmospheric CO_2.

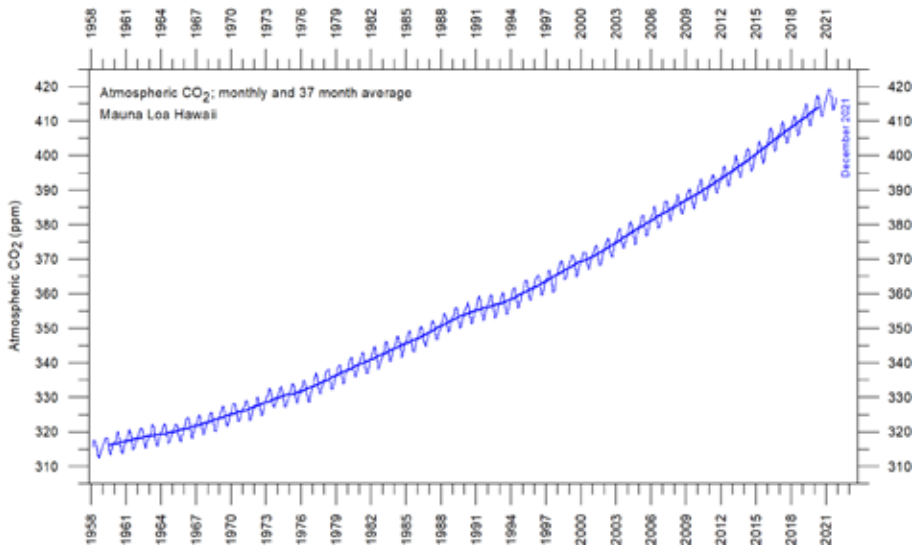

Figure 18: The Mauna Loa CO_2 record

Thin lines: monthly value; thick lines: 37-month running mean.

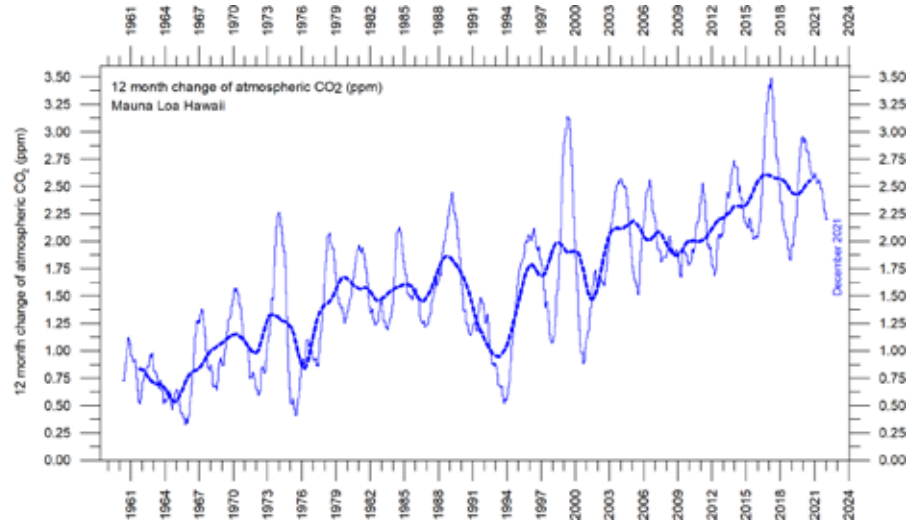

Figure 19: Annual CO_2 change

Difference of two 12-month averages. Thin lines: monthly value; thick lines: 3-year running mean.

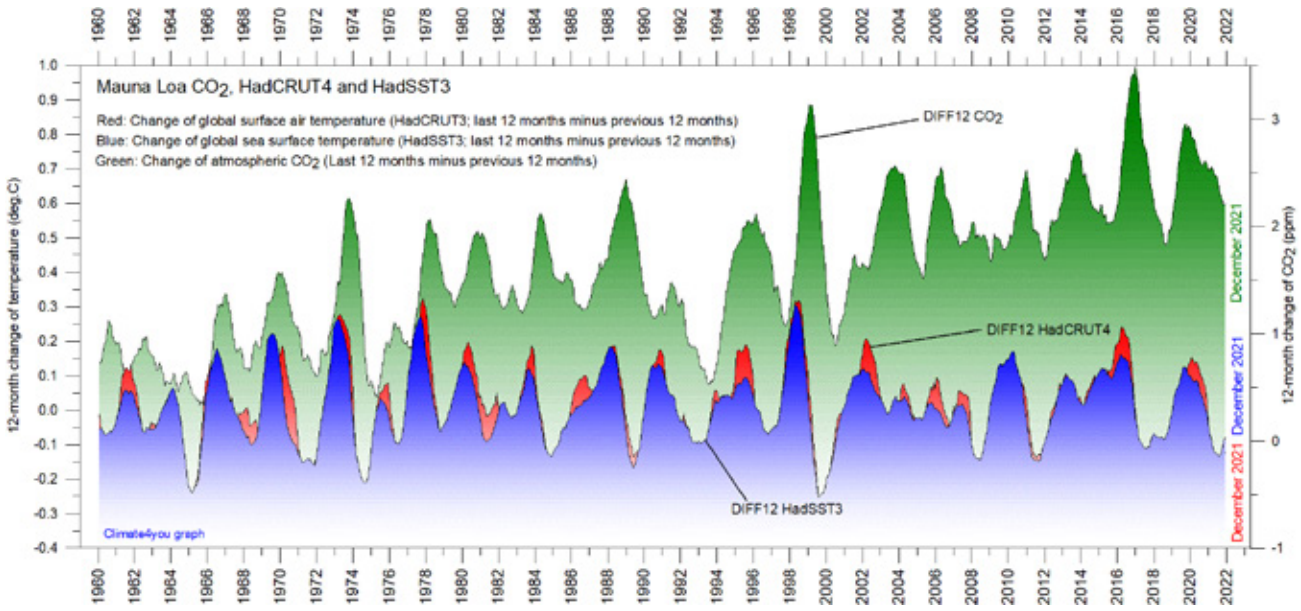

Figure 20: Correlation of carbon dioxide concentrations and temperature records.

Annual (12-month) change of global atmospheric CO_2 concentration (Mauna Loa; green), global sea surface temperature (HadSST3; blue) and global surface air temperature (HadCRUT4; red). All graphs are showing monthly values of DIFF12, the difference between the average of the last 12 months and the average for the previous 12 months for each data series.

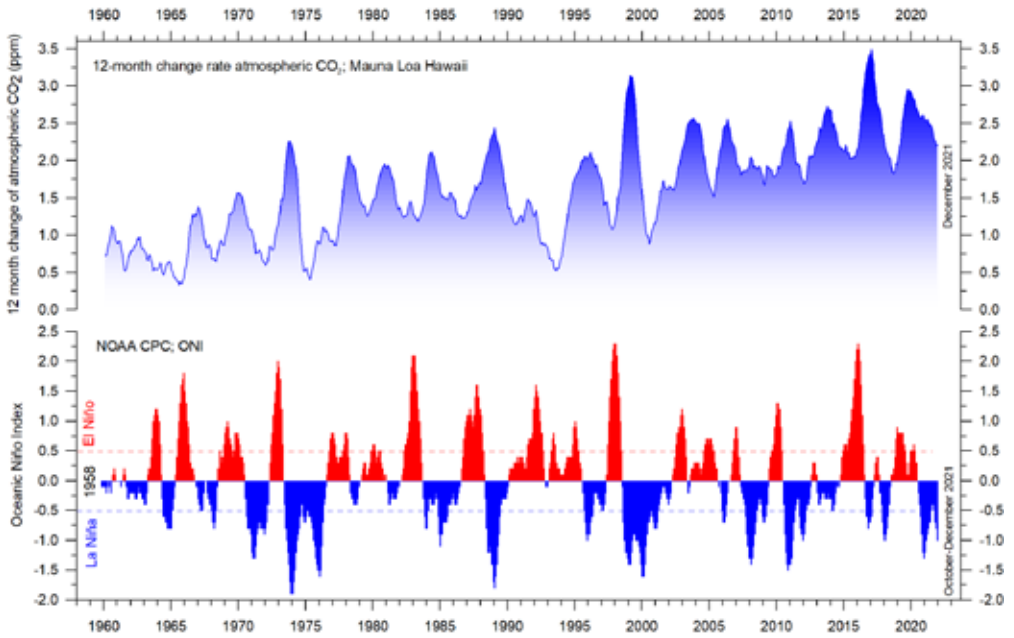

Figure 21: CO_2 growth and El Niño and La Niña episodes

Visual association between annual growth rate of atmospheric CO_2 (upper panel) and Oceanic Niño Index (lower panel).

3. Ocean temperatures

Recent surface temperature anomalies

The three maps in Figure 22 show the nearly neutral situation at the end of December 2019, followed by a moderate La Niña in much of 2020 and 2021.

Figure 23 shows all El Niño and La Niña episodes since 1950. The recent 2015–16 El Niño episode was among the strongest since the beginning of the record in 1950. Considering the entire record, however, recent variations between El Niño and La Niña episodes do not appear abnormal.

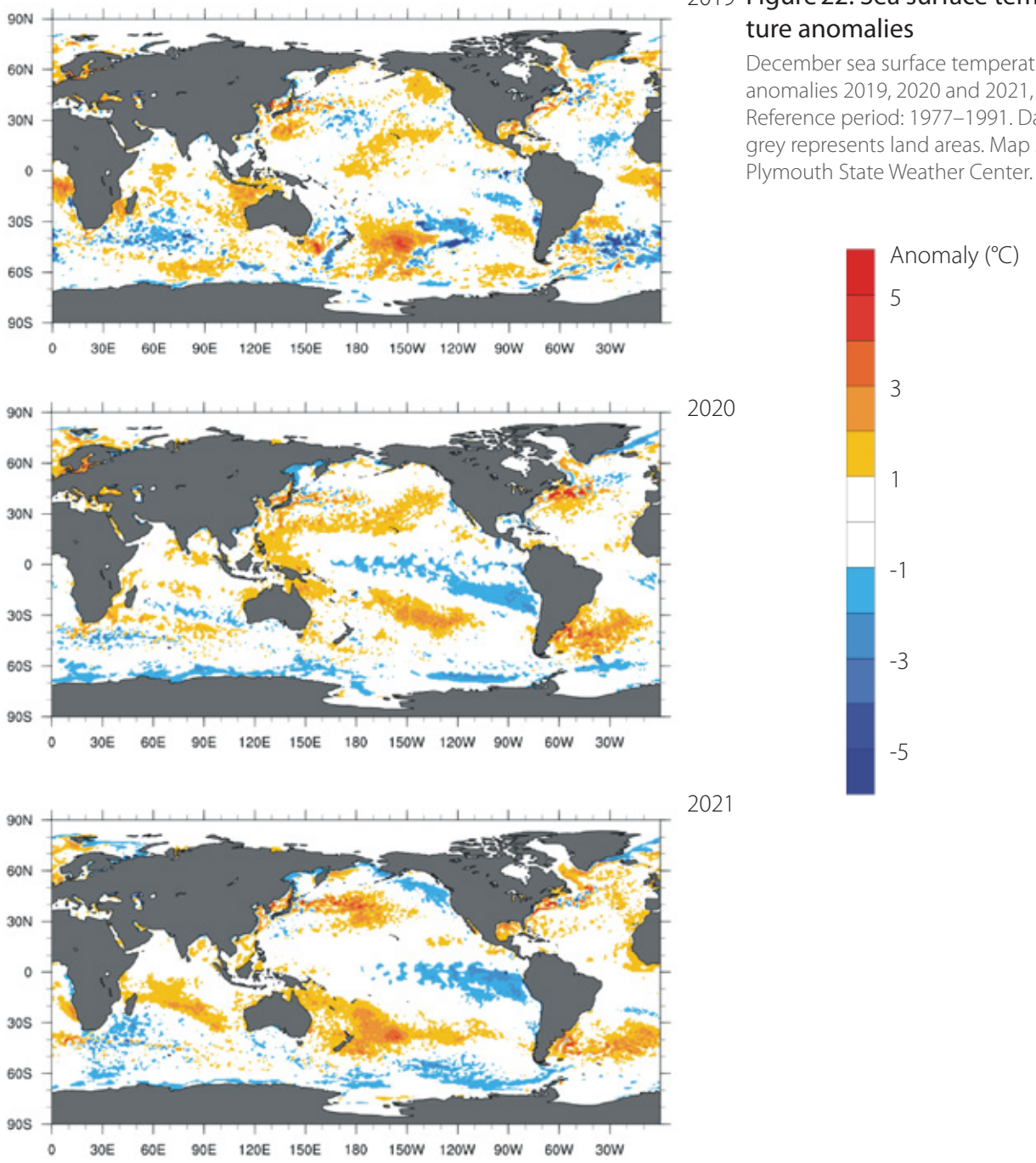

Figure 22: Sea surface temperature anomalies

December sea surface temperature anomalies 2019, 2020 and 2021, (°C). Reference period: 1977–1991. Dark grey represents land areas. Map source: Plymouth State Weather Center.

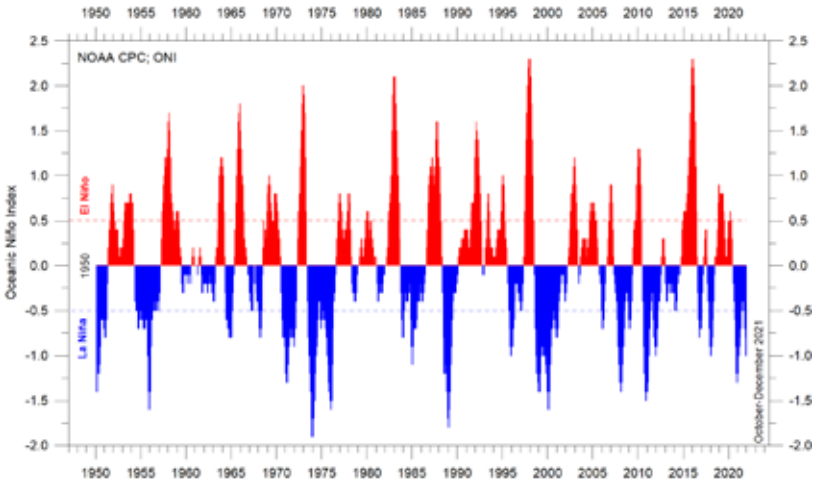

Figure 23: The El Niño index

Warm and cold episodes for the Oceanic Niño Index (ONI), defined as 3-month running mean of ERSST.v5 SST anomalies in the Niño 3.4 region (5°N-5°S, 120°-170°W). Anomalies are centred on 30-year base periods updated every 5 years.

By latitude

Figure 24, which is based on observations by Argo floats (Roemmich and Gilson 2009), shows that, on average, the temperature of the global oceans down to 1900 m depth has been increasing since about 2010. Since 2013, this increase has predominantly been due to changes occurring near the Equator, between 30°N and 30°S. In contrast, for the circum-Arctic oceans north of 55°N, depth-integrated ocean temperatures have been decreasing since 2011. Near the Antarctic, south of 55°S, temperatures have essentially been stable. At most latitudes, a clear annual rhythm is seen.

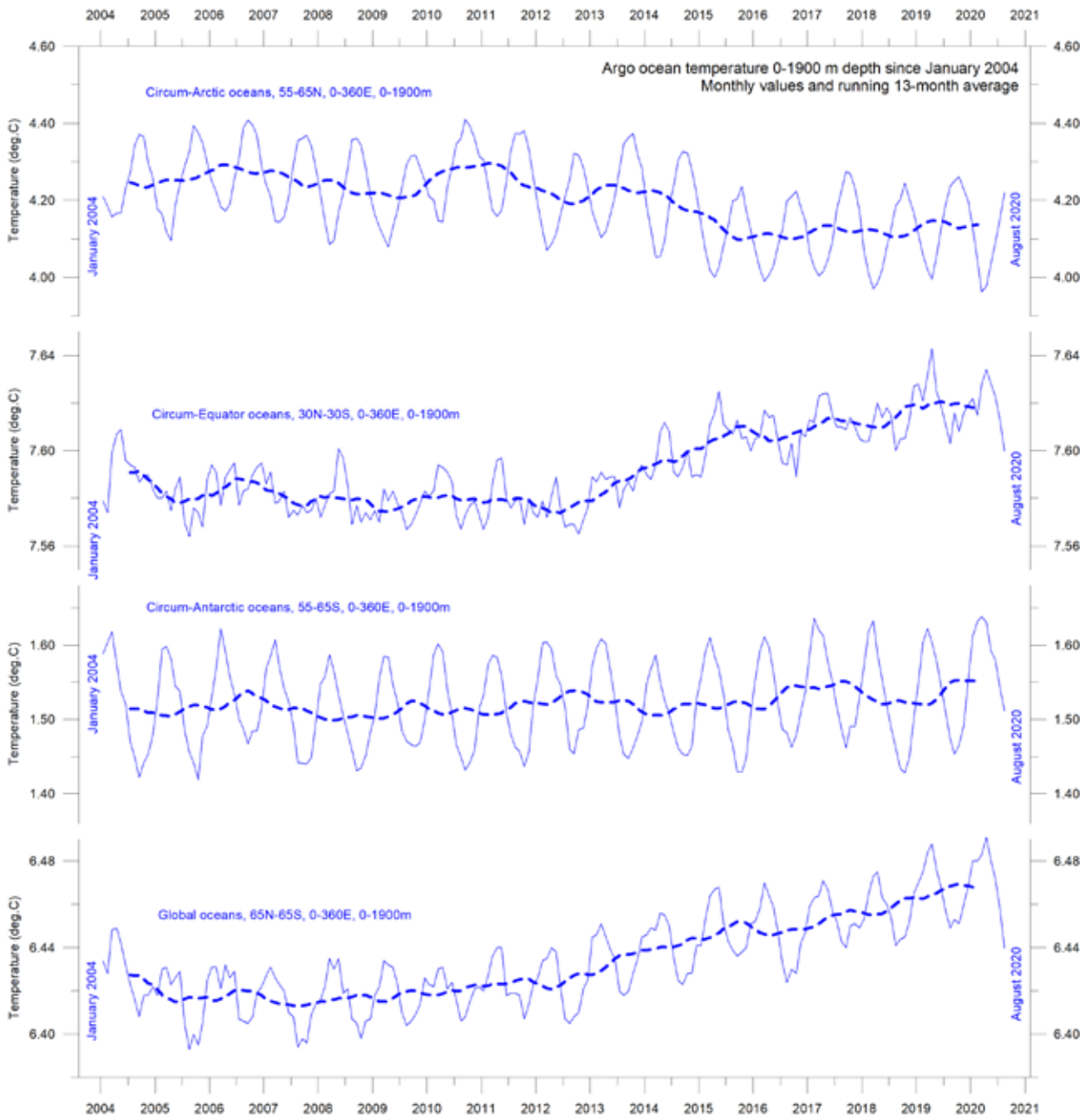

Figure 24: Ocean temperatures to 1900 m

Average ocean temperatures January 2004–August 2020 at 0–1900 m depth in selected latitudinal bands, using Argo data. The thin line shows monthly values, and the thick dotted line shows the running 13-month average. Source: Global Marine Argo Atlas.

By depth

Figure 25 shows global average oceanic temperatures at different depths. An annual rhythm can be seen down to about 100 m depth. In the uppermost 100 m, temperatures have increased since about 2011. At 200–400 m depth, temperatures have exhibited little change during the observational period. For water depths below 400 m, however, temperatures are again seen to be increasing. Interestingly, the diagram suggests that this increase first commenced at 1900 m depth in around 2009, and from there has been gradually spreading upwards. At 600 m depth, the present temperature increase began around 2012; that is, about three years later than at 1900 m depth. The timing of these changes shows that average temperatures in the upper 1900 m of the oceans are not only influenced by conditions playing out at or near the ocean surface, but also by processes operating at depths greater than 1900 m. Part of the present ocean warming therefore appears to be due to circulation features operating at great depths, and not directly related to processes operating at or near the surface.

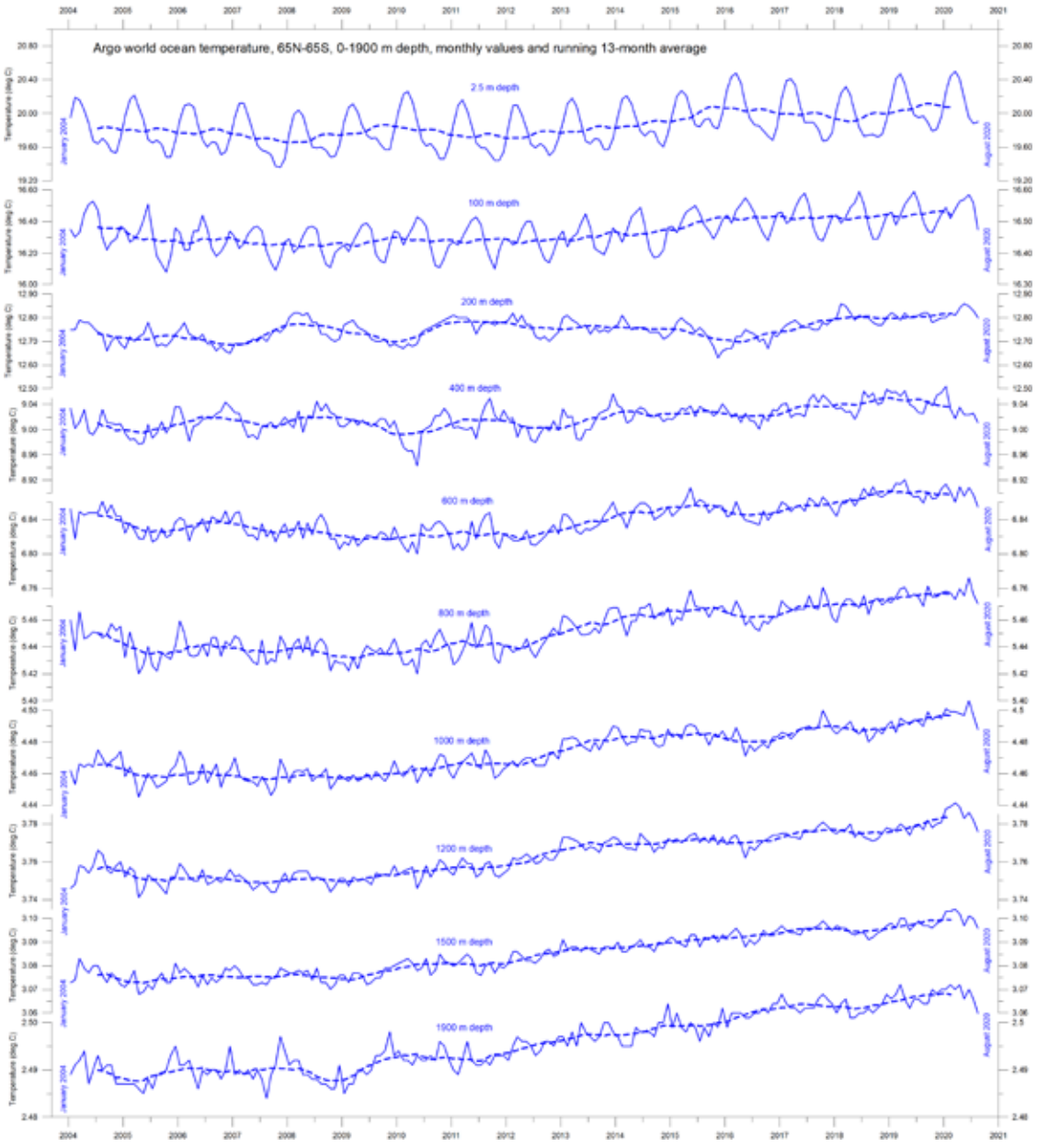

Figure 25: Ocean temperatures at different depths

Ocean temperatures January 2004–August 2020 at different depths between 65°N and 65°S, using Argo data. The thin line shows monthly values, and the dotted line shows the running 13-month average. Source: Global Marine Argo Atlas.

This is also visible in Figure 26, which shows the net change of global ocean temperatures at different depths, calculated as the difference between the 12-month averages of January–December 2004 and September 2019–August 2020, respectively. The largest net changes are seen to have occurred in the uppermost 200 m of the water column. However, average values, as shown in this diagram, although important, also hide many interesting regional details (Figure 27).

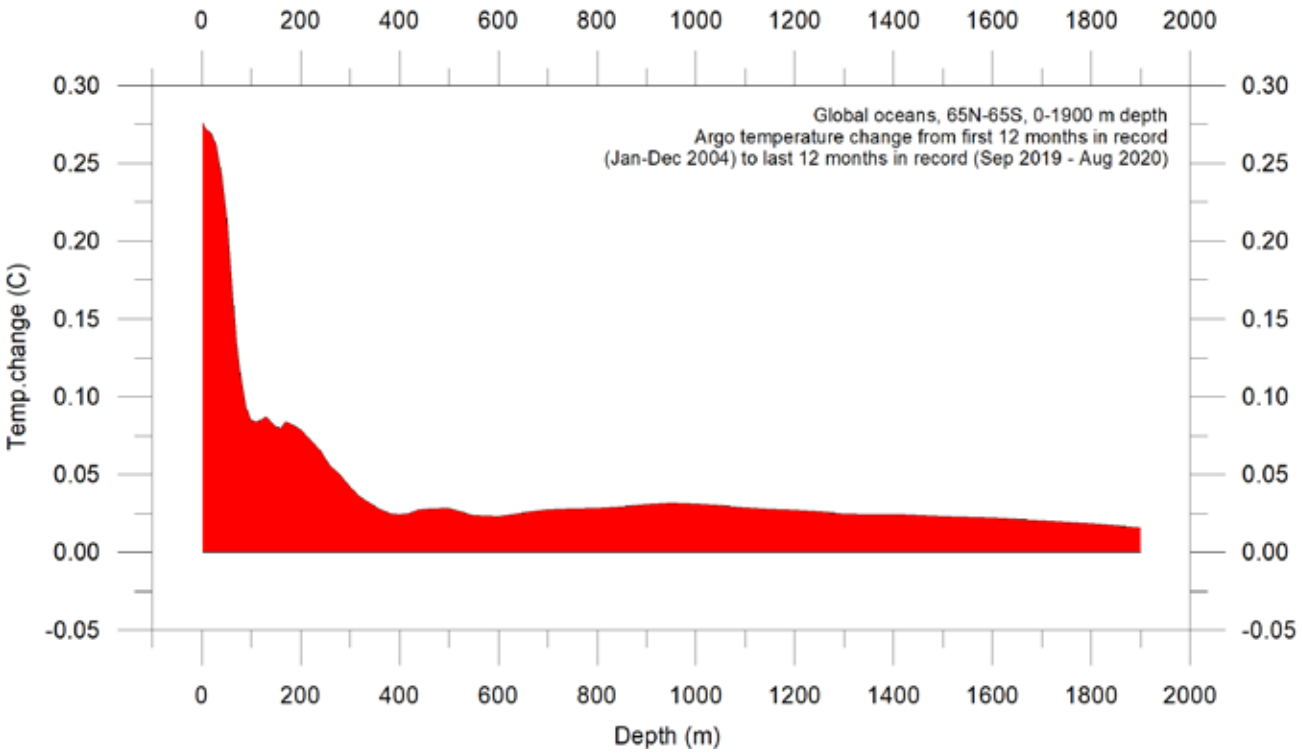

Figure 26: Temperature changes 0–1900 m

Global ocean net temperature change since 2004 from surface to 1900 m depth, using Argo-data. Source: Global Marine Argo Atlas.

By region and depth

Figure 27 shows the latitudinal variation of oceanic temperature net changes between January-December 2004 and September 2019–August 2020 for various depths, calculated as in Figure 26. The three panels show the net change in Arctic Oceans (55–65°N), Equatorial Oceans (30N-30°S), and Antarctic Oceans (55–65°S), respectively.

The global net surface warming displayed by Figure 26 affects the Equatorial and Antarctic Oceans, but not the Arctic Oceans (Figure 27). In reality, net cooling is pronounced down to 1400 m for the northern oceans. However, a major part of Earth's land areas is in the Northern Hemisphere, so the surface area (and volume) of the 'Arctic' oceans is much smaller than the 'Antarctic' oceans, which in turn is smaller than the 'Equatorial' oceans. In fact, half of the planet's surface area (land and ocean) is located between 30°N and 30°S. Nevertheless, the contrast in net temperature changes experienced over the period 2004–2020 for the different latitudinal bands is instructive. For the two Polar Oceans, the Argo data appear to demonstrate the existence of a bi-polar seesaw, as described by Chylek et al. (2010). It is no less interesting that the trend in the near-surface ocean temperature in the two Polar Oceans contrasts with the overall development of sea ice in the two polar regions (see later in this report).

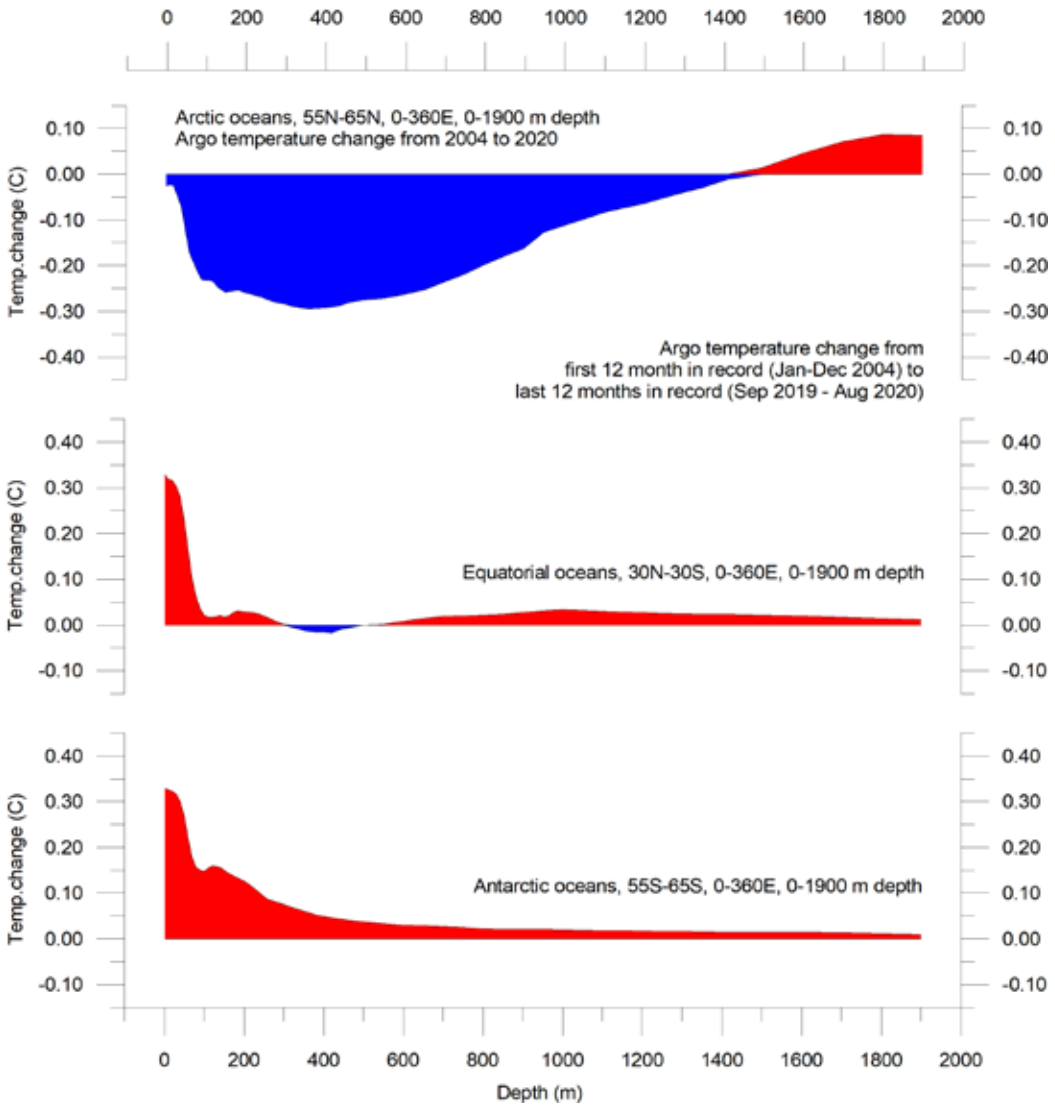

Figure 27: Temperature changes 0–1900 m

Global ocean net temperature change since 2004 from surface to 1900 m depth. Source: Global Marine Argo Atlas.

Ocean temperature net change 2004–2020 in selected sectors

Figure 29a shows net temperature changes between 2004 and 2019 along a transect of the oceans located at 20°W, corresponding to the Atlantic Ocean. To prepare the diagram, annual average ocean temperatures for 2019 and 2004 were compared, the latter representing the first 12 months of the Argo-record. However, the Argo data portal Global Argo Marine Atlas is, at time of writing, only updated to August 2020, so to give an insight into the most recent changes, the 12-month net change from September 2019 to August 2020 is shown in Figure 29b. Warm colours indicate net warming from 2004 to 2019 and from September 2019 to August 2020, and blue colours indicate cooling. Due to the spherical shape of the Earth, northern and southern latitudes represent only small ocean volumes, compared to latitudes near the Equator. With this reservation in mind, the two parts of the Figure nevertheless reveal several interesting features.

The most prominent feature in the Atlantic profile for 2004–2019 is a marked net cooling at the surface north of the Equator, especially north of 45°N, where deeper layers (down to 1500 m) are also involved. At and south of the Equator, net warming dominates at the surface, although net cooling dominates at 50–300 m. The maximum Atlantic Ocean net warming over 2004–2019 has taken place between 5°N and

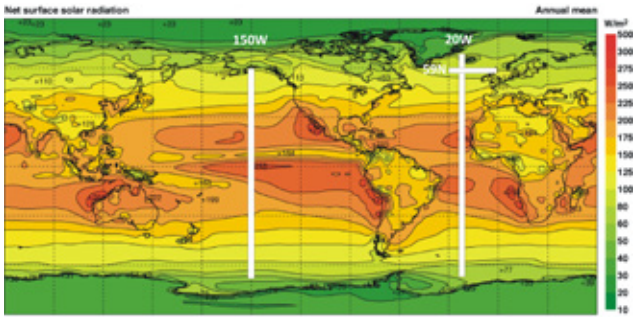

Figure 28: Location of the three profiles

Average annual mean net surface solar radiation (W/m²), and the location of three profiles shown and discussed below.

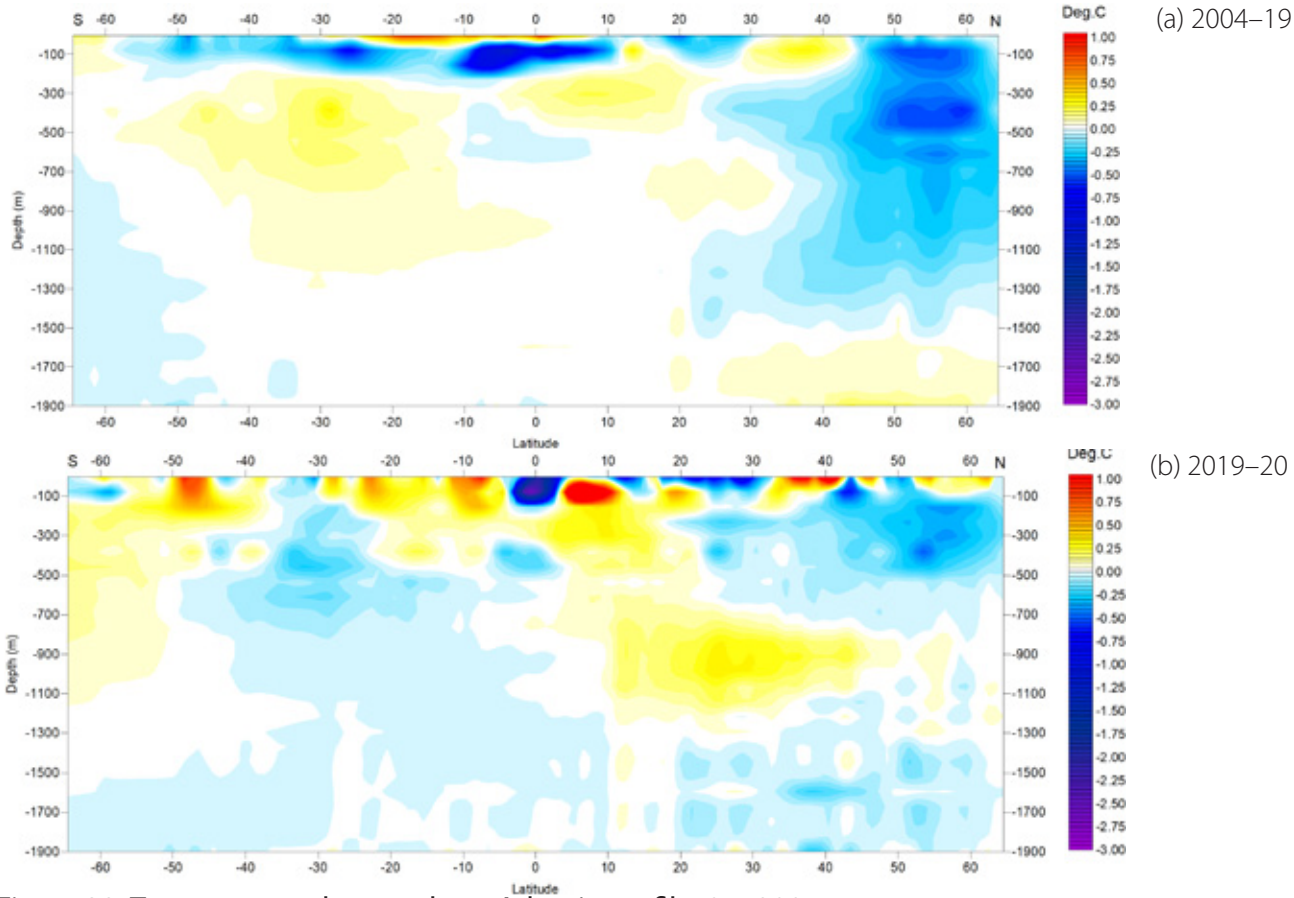

Figure 29: Temperature change along Atlantic profile, 0–1900 m

(a) 2004–2019 and (b) Sept 19–Aug 20. See Figure 27 for geographical location of transect. Data source: Global Marine Argo Atlas.

25°S, affecting shallow water depths (to about 50 m). Warming also affects latitudes between 10°S and 45°S, between 200 and 1200 m depth. The temperature development over the last 12 months on record (Figure 29b) is more complicated, especially near the surface. However, the South Atlantic warming at depth appears to be weakening over the last 12 months of the record, while the North Atlantic cooling appears to be continuing, with the exception of depths between 800 and 1100 m.

Of special interest is the temperature dynamics displayed within a 59°N transect across the North Atlantic Current, shortly south of the Faroe Islands, as this is important for weather and climate in much of Europe. Figure 30 shows a time series at 59°N, from 30°W to 0°W, from the surface to 800 m water depth, basically representing a section across the water masses affected by the North Atlantic Current. Ocean temperatures higher than 9°C are shown as red colours.

This time series, although still relatively short, displays noteworthy dynamics. The importance of warm water (above 9°C) apparently peaked in early 2006 and was followed by a gradual reduction until 2016. Since then, a partial temperature recovery has taken place in the section considered. The observed change, from high peak to low peak, playing out over approximately 11 years, might suggest the existence of a cycle of about 22-years' duration, but we will have to wait until the Argo series is longer before drawing firm conclusions.

Figure 31 is the same data series (59°N, 30–0°W, 0–800 m depth, 2004–2020), but now displayed as a graph of depth-integrated average ocean temperature.

Figure 32 shows two equivalent diagrams for the Pacific Ocean, showing the net changes

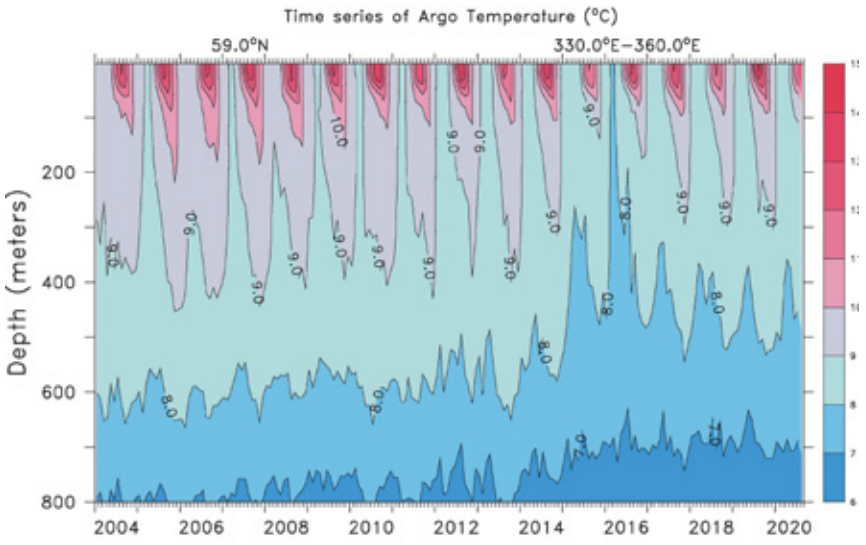

Figure 30: Temperature change along North Atlantic Current profile, 0–800 m

See Figure 28 for geographical location of transect. Data source: Global Marine Argo Atlas.

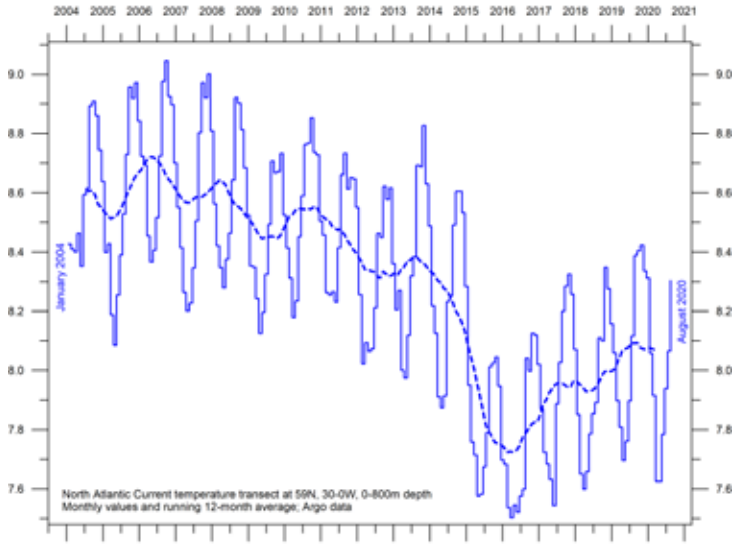

Figure 31: Depth-integrated temperature for the North Atlantic Current profile

See Figure 28 for geographical location of transect. Data source: Global Marine Argo Atlas.

from 2004 to 2019/20 along 150°W, prepared in the same way as the Atlantic diagrams above. Warm colours indicate net warming, and blue colours net cooling. Again, northern and southern latitudes represent only relatively small ocean volumes, compared to latitudes near the Equator.

One interesting feature for 2004–2019 (Figure 32a) is a slight net cooling south of 55°S, affecting nearly all water depths down to 1900 m. This contrasts with an overall net warming down to 1000 m depth north of 55°S. Net warming has been especially prominent between 40°N and 60°N, down to 200 m depth. In contrast, net cooling characterises depths between 100 and 500 m depth between 5°S and 30°N, and between 20°S and 30°S. During the last 12 months of the Argo record (Figure 32b), cooling is seen to dominate all depths between 45°S and 30°N. At least part of this recent temperature development can probably be related to the onset of La Niña towards the end of 2020 (Figure 23).

Neither of the Atlantic and Pacific longitudinal diagrams above show to what extent the changes displayed are caused by ocean dynamics operating east and west of the two profiles considered; they only display the net changes between 2004 and 2019/20 along the longitudes chosen. For that reason, the diagrams should not be overinterpreted. However, the two longitudinal profiles have an interesting contrast, with the Pacific Ocean mainly warming, and especially north of Equator, and cooling in the south, while the opposite is true of the Atlantic profile: cooling in the north and warming in the south.

(a) 2004–19

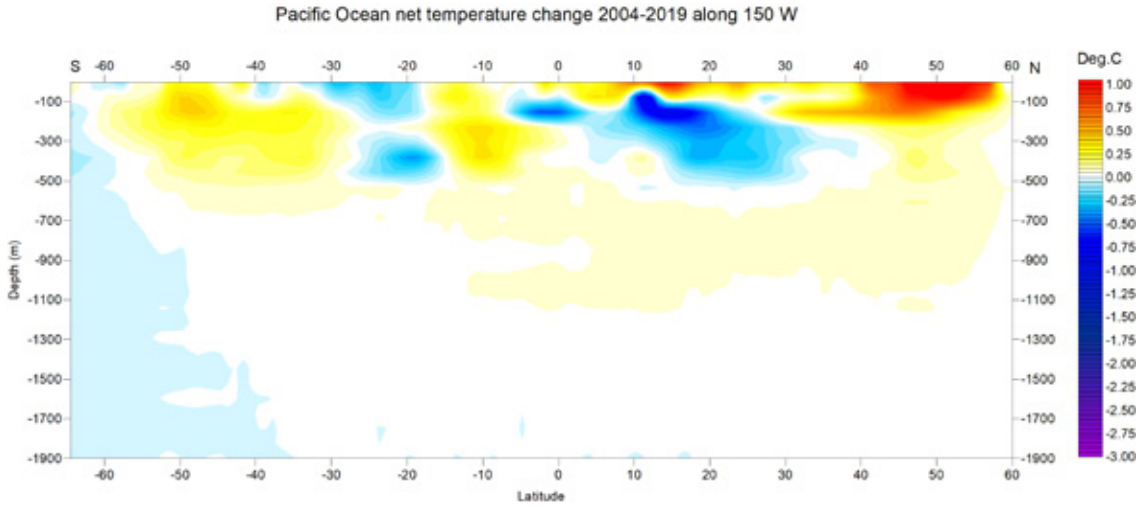

(b) 2019–20

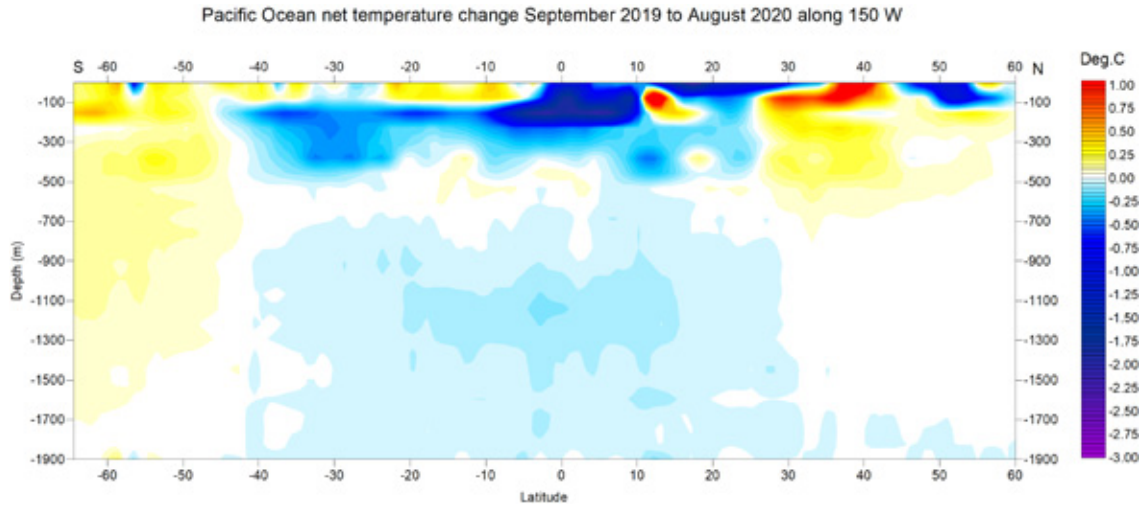

Figure 32: Temperature change along Pacific profile, 0–1900 m

(a) 2004–2019 and (b) Sept 19–Aug 20. See Figure 28 for geographical location of transect. Data source: Global Marine Argo Atlas.

4. Ocean oscillations

Southern Oscillation Index

The Southern Oscillation Index (SOI) is calculated from the monthly or seasonal fluctuations in the air pressure difference between Tahiti and Darwin. Sustained negative values of the SOI (Figure 33) often indicate El Niño episodes. Such negative values are usually accompanied by persistent warming of the central and eastern tropical Pacific Ocean, a decrease in the strength of the Pacific Trade Winds, and a reduction in rainfall over eastern and northern Australia.

Positive values of the SOI are usually associated with stronger Pacific trade winds and higher sea surface temperatures to the north of Australia, indicating La Niña episodes. Waters in the central and eastern tropical Pacific Ocean become cooler at such times, and Eastern and northern Australia usually receive increased precipitation.

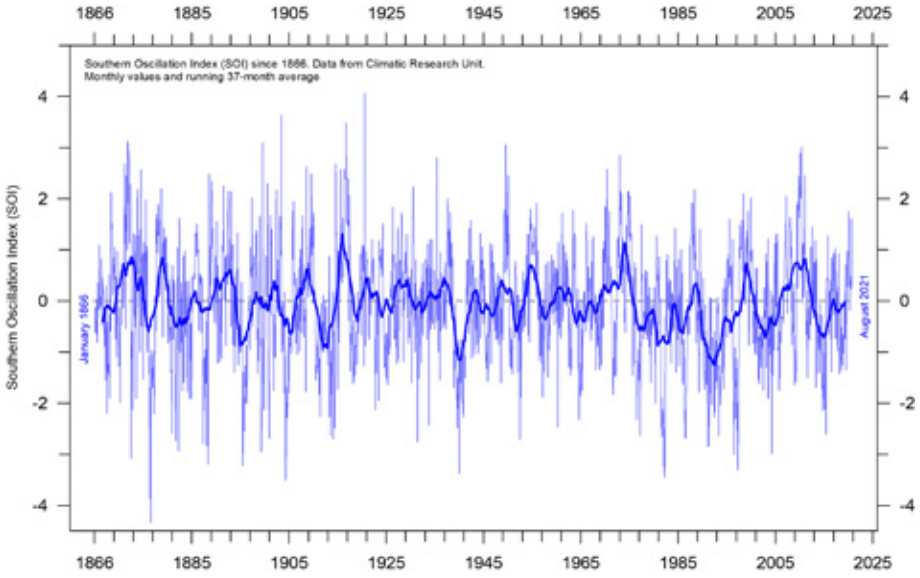

Figure 33: Annual SOI anomaly since 1866

The thin line represents annual values, while the thick line is the simple running 5-year average. Source: Climatic Research Unit, University of East Anglia.

Pacific Decadal Oscillation

The PDO (Figure 34) is a long-lived El Niño-like pattern of Pacific climate variability, with data extending back to January 1900. Its causes are not currently known, but even in the absence of a theoretical understanding, PDO climate information improves season-to-season and year-to-year climate forecasts for North America because of its strong tendency for multi-season and multi-year persistence. The PDO also appears to be roughly in phase with global temperature changes. Thus, from a societal impact perspective, recognition of the PDO is important because it shows that 'normal' climate conditions can vary over time periods comparable to a human lifespan.

The PDO illustrates how global temperatures are tied to sea surface temperatures in the Pacific, the largest ocean on Earth. When sea surface temperatures are relatively low (negative phase PDO), as from 1945 to 1977, global air temperature decreases. When sea surface temperatures are high (positive phase PDO), as from 1977 to 1998, global surface air temperature increases (Figure 7).

A Fourier frequency analysis (not shown here) shows the PDO record to be influenced by a 5.7-year cycle, and possibly also by a longer one of about 53 years' duration.

Atlantic Multidecadal Oscillation

The Atlantic Multidecadal Oscillation (AMO; Figure 35) is a mode of variability occurring in the North Atlantic Ocean sea surface temperature field. The AMO is basically an index of North Atlantic sea surface temperatures (SSTs).

The AMO index appears to be correlated to

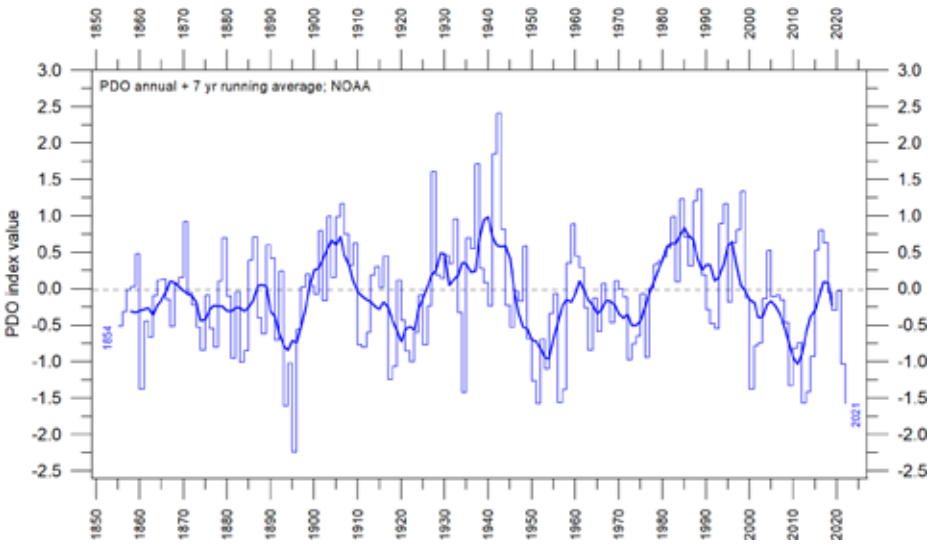

Figure 34: Annual values of the Pacific Decadal Oscillation (PDO) according to the Physical Sciences Laboratory, NOAA.

The thin line shows the annual PDO values, and the thick line is the simple running 7-year average. Source: PDO values from NOAA Physical Sciences Laboratory: ERSST V5 https://psl.noaa.gov/pdo/

air temperatures and rainfall over much of the Northern Hemisphere. The association appears to be high for North Eastern Brazil, African Sahel rainfall and North American and European summer climate. The AMO index also appears to be associated with changes in the frequency of North American droughts and is reflected in the frequency of severe Atlantic hurricanes.

As one example, the AMO index may be related to the past occurrence of major droughts in the US Midwest and the Southwest. When the AMO is high, these droughts tend to be more frequent or prolonged, and vice-versa for low values of AMO. Two of the most severe droughts of the 20th century in the US occurred during the peak AMO values between 1925 and 1965: The Dust Bowl of the 1930s and the 1950s droughts. On the other hand, Florida and the Pacific Northwest tend to be the opposite; high AMO is here associated with relatively high precipitation.

A Fourier-analysis (not shown here) show the AMO record to be controlled by an about 67-year long cycle, and to a lesser degree by a 3.5-year cycle.

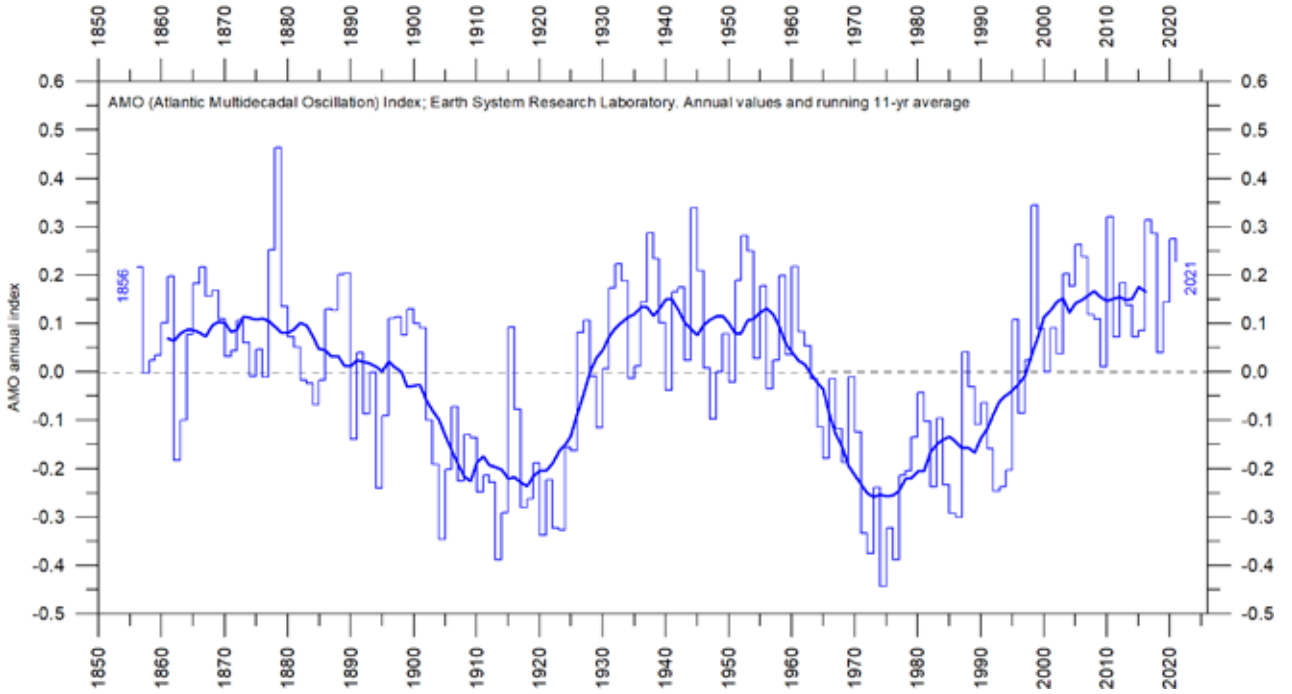

Figure 35: The Atlantic Multidecadal Oscillation

Annual Atlantic Multidecadal Oscillation (AMO) detrended and unsmoothed index values since 1856. The thin blue line shows annual values, and the thick line is the simple running 11-year average. Data source: Earth System Research Laboratory, NOAA, USA.

5. Sea-level

In general

Global, regional, and local sea levels always change. During the last glacial maximum, about 20–25,000 years ago, global sea level was around 120 m lower than today. Since the end of the so-called Little Ice Age, about 100–150 years ago, the global sea level has on average increased by 1–2 mm/year, according to tide gauges located at coasts. Observed data from tide gauges worldwide can be accessed from the PSMSL Data Explorer (see link at the end of this report).

Global (or eustatic) sea-level change is measured relative to an idealised reference level, the geoid, which is a mathematical model of planet Earth's surface (Carter et al. 2014). Global sea-level is a function of the volume of the ocean basins and the volume of water they contain. Changes in global sea-level are caused by – but not limited to – four main mechanisms:

- Changes in local and regional air pressure and wind, and tidal changes introduced by the Moon.
- Changes in ocean basin volume by tectonic (geological) forces.
- Changes in ocean water density caused by variations in currents, water temperature and salinity.
- Changes in the volume of water caused by changes in the mass balance of terrestrial glaciers.

In addition, mechanisms such as storage of ground water, storage in lakes and rivers, evaporation also affect sea level.

Ocean basin volume changes occur too slowly to be significant over human lifetimes and it is therefore mechanisms 3 and 4 that drive contemporary concerns about sea-level rise.

Higher temperature in itself is only a minor factor contributing to global sea-level rise, because seawater has a relatively small coefficient of expansion and because, over the timescales of interest, any warming is largely confined to the upper few hundred metres of the ocean surface.

The growth and decay of floating glaciers has no influence on sea level. However, the melting of land-based ice – including both mountain glaciers and the ice sheets of Greenland and Antarctica – is a more significant driver. For example, during the glacial–interglacial climatic cycling over the last half-million years, sea-levels were about 120 m lower than today. Moreover, during the most recent interglacial, about 120,000 years ago, global temperature was higher than today, and significant extra parts of the Greenland ice sheet melted. As a consequence, global sea-level was several metres higher than today.

On a regional and local scale, however, factors relating to changes in air pressure, wind and geoid must also be considered. As an example, changes in the volume of the Greenlandic Ice Sheet will affect the geoid in the regions adjacent to Greenland. Should overall mass in Greenland diminish, the geoid surface will be displaced in direction of the planet's centre, and sea level in the regions neighbouring Greenland will drop. This will happen even though the overall volume of water in the global oceans increases as a result of the net loss of glacier ice.

In northern Europe, another factor must also be considered when estimating the future sea level. Norway, Sweden, Finland, and Denmark were all totally or partly covered by the European Ice Sheet 20–25,000 years ago. Even today, the effect of this ice load is clearly demonstrated by the fact that most of this region experiences an ongoing isostatic land rise of several millimetres per year. At many sites, this more than compensates for the slow global sea-level rise, so a net sea-level drop in relation to the land is recorded.

The relative movement of sea level in relation to land is what matters for coastal planning and is termed the relative sea level change. This is what is recorded by tide gauges.

From satellite altimetry

Satellite altimetry is a relatively new type of measurement, providing unique and valuable insights into the detailed surface topography of the oceans, and how it is changing, with nearly global coverage. However, it is probably not a precise tool for estimating absolute changes in global sea level due to assumptions made when interpreting the original satellite data.

One of the assumptions made during the conversion of satellite altimetry data into sea-level change estimates (Figure 36) is the Glacial Isostatic Adjustment (GIA). This relates to large-scale, long-term mass transfer from the oceans to the land, in the form of rhythmic waxing and waning of the large Quaternary ice sheets in North America and North Europe. This enormous mass transfer causes cyclical changes in surface load, resulting in viscoelastic mantle flow and elastic effects in the upper crust. However, we have inadequate knowledge to give rigorous estimates of how much this affects sea-level estimates: it depends upon how the Earth's crust-mantle and the deglaciation after the last ice age are modelled. Because of this (and additional factors), interpretations on modern global sea-level change based on satellite altimetry vary somewhat. In Figure 36, the global sea-level rise estimate is about 3.3 mm/year, with the estimated GIA effect removed.

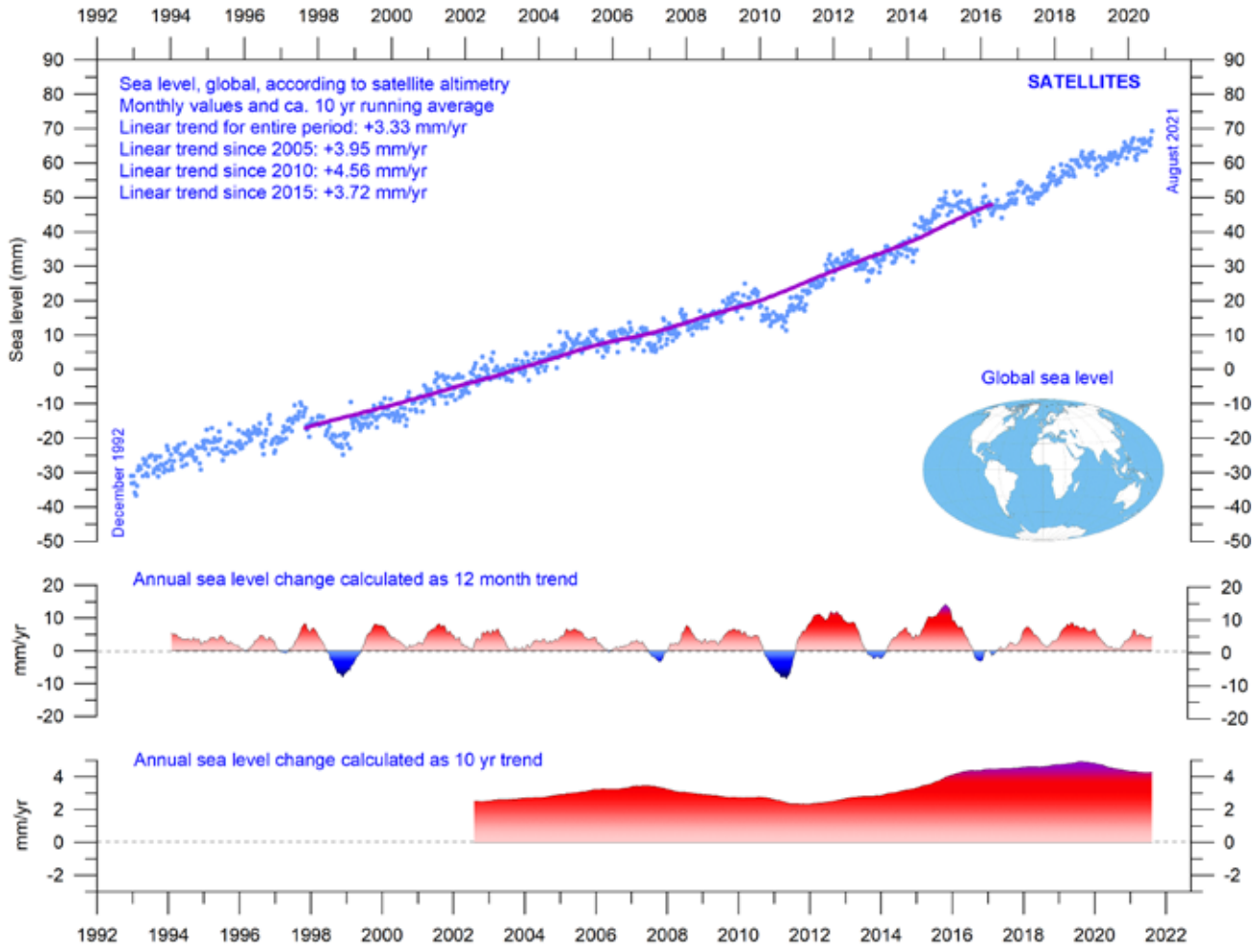

Figure 36: Global sea level change since December 1992

The two lower panels show the annual sea level change, calculated for 1- and 10-year time windows, respectively. These values are plotted at the end of the interval considered. Source: Colorado Center for Astrodynamics Research at University of Colorado at Boulder. The blue dots are the individual observations (with calculated GIA effect removed), and the purple line represents the running 121-month (ca. 10-year) average.

From tide gauges

Tide gauges are located directly at coastal sites and record the net movement of the local ocean surface in relation to land (Figure 37). Measurements of local relative sea-level change (see, for example, Figure 38) are the key information for coastal planning, and it is tide-gauge rather than satellite data that are relevant for this purpose.

In a precise context, the measured net movement of the local coastal sea-level comprises two local components:

- the vertical change of the ocean surface
- the vertical change of the land surface.

For example, a tide-gauge may record an apparent sea-level increase of 3 mm/year. If geodetic measurements show the land to be sinking by 2 mm/year, the real sea-level rise is only 1 mm/year (3 minus 2 mm/year). In a global context, the value of 1 mm/year is relevant, but in a local coastal planning context, it is the 3 mm/year tide-gauge figure that should be considered by local authorities.

To construct time series of sea-level measurements at each tide gauge, the monthly and annual means must be reduced to a common datum. This reduction is performed by the *Permanent Service for Mean Sea Level* (PSMSL), making use of the tide-gauge datum history provided by supplying national authorities. The Revised Local Reference (RLR) datum at each station is defined to be approximately 7000 mm below mean sea level, with this arbitrary choice made many years ago to avoid negative numbers in the resulting RLR data.

Few places on Earth are completely stable, and most tide gauges are located at sites exposed to tectonic uplift or sinking (the vertical change of the land surface). This widespread vertical instability has several causes, and affects the interpretation of data from the individual tide gauges. Much effort is therefore put into correcting for local tectonic movements.

Data from tide gauges from tectonically

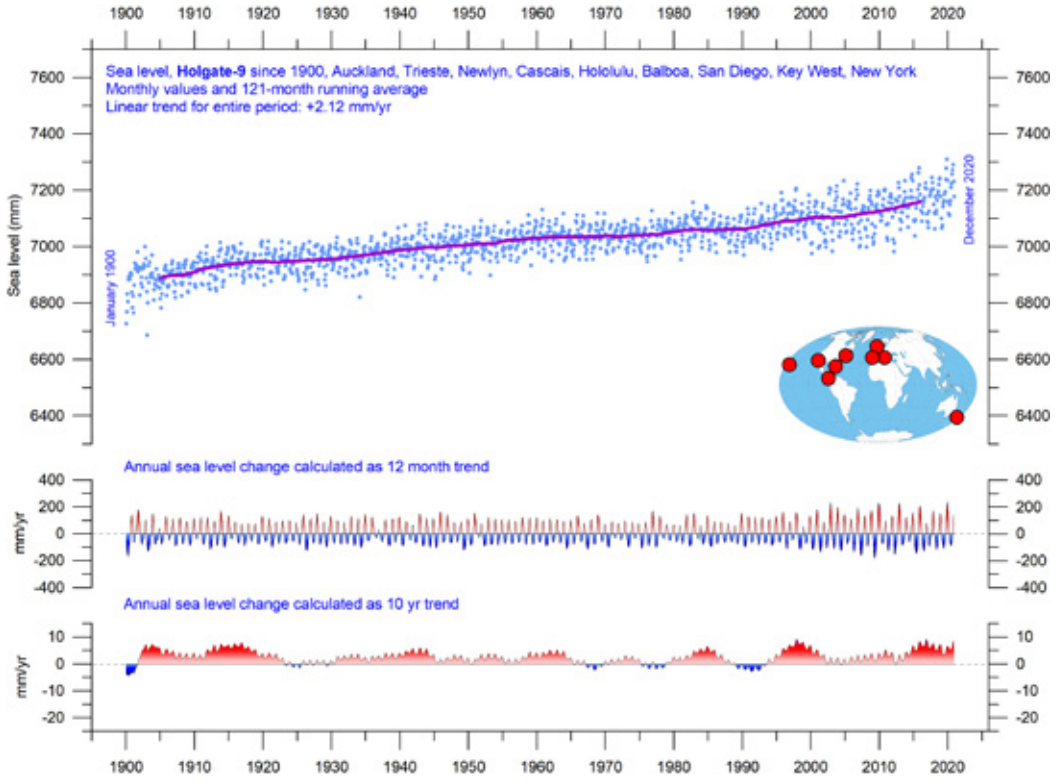

Figure 37: Holgate-9 monthly tide gauge data from PSMSL Data Explorer

The Holgate-9 are a series of tide gauges located in geologically stable sites. The two lower panels show the annual sea level change, calculated for 1- and 10-year time windows, respectively. These values are plotted at the end of the interval considered. Source: Colorado Center for Astrodynamics Research at University of Colorado at Boulder. The blue dots are the individual observations, and the purple line represents the running 121-month (ca. 10-year) average.

stable sites is therefore of particular interest. One example of a long record obtained from such a site is shown in Figure 38 (Korsør, Denmark, since January 1897). This record indicates a stable sea-level rise of about 0.83 mm/year, without any indication of recent acceleration.

Data from tide-gauges all over the world suggest an average global sea-level rise of 1–2 mm/year, while the satellite-derived record (Figure 36) suggests a rise of about 3.3 mm/year, or more. The noticeable difference (a ratio of about 1:2) between the two datasets is remarkable, but has no generally accepted explanation. It is, however, known that satellite observations face complications in coastal areas. Vignudelli et al. (2019) provide an updated overview of the current limitations of classical satellite altimetry in coastal regions.

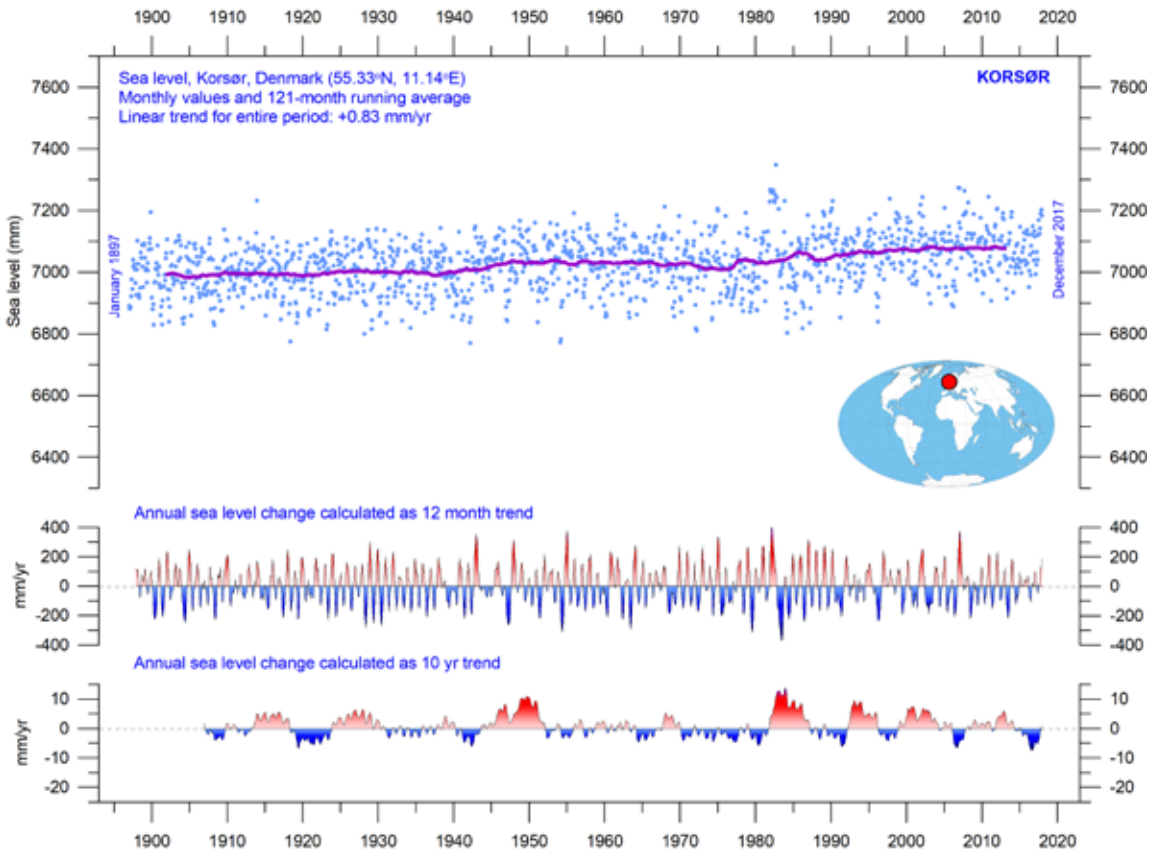

Figure 38: Korsør (Denmark) monthly tide gauge data

From PSMSL Data Explorer. The blue dots are the individual monthly observations, and the purple line represents the running 121-month (ca. 10-year) average. The two lower panels show the annual sea level change, calculated for 1- and 10-year time windows, respectively. These values are plotted at the end of the interval considered.

Modelled for the future

The issue of sea-level change, and in particular the identification of a hypothetical human contribution to it, is a complex topic. Given the scientific and political controversy that surrounds the matter, public interest is entirely understandable.

A recent IPCC publication, the 6th Assessment Report from Working Group I, was released on 9 August 2021. Data regarding global and regional sea-level projections 2020–2150 are available from the IPCC AR6 Sea Level Projection Tool (see link at the end of this report). This is the output of models, taking into account factors such as glacier mass change, vertical land movement, water temperature and storage. The projections, for different carbon dioxide emissions scenarios, are calculated relative to a baseline defined by observations from 1995 to 2014.

It is enlightening to compare the model output with observed sea-level data, as illustrated in Figure 39 for Oslo and Copenhagen. Both Norway and Denmark were totally or partly covered by the European Ice Sheet 20–25,000 years ago. Even today, the effect of this ice load is clearly seen in the fact that southern Norway experiences an ongoing isostatic land rise of several millimetres per year, while Denmark is not affected to the same degree. At many sites, this isostatic movement more than compensates for the slow global sea-level rise, so a net sea-level decrease in relation to land is recorded.

Oslo was covered by thick ice during the last glaciation and is therefore affected by a rather marked isostatic land rise today. If the observed sea-level change rate at Oslo continues (based on more than 100 years of observations), the relative sea level at Oslo (in relation to land) will have dropped by about 28 cm by year 2100, compared to now (Figure 39). In contrast, according to IPCC, the modelled relative sea level (in relation to land) at Oslo will have increased about 17 cm by year 2100, compared to now. Sea-level increase is supposed to begin rather suddenly around 2020 at Oslo, in contrast to the previous sea-level decrease of about -3.44 mm/year recorded since 1914.

Denmark was near the margin of the European Ice Sheet during the last glacial maximum, and the observed relative sea-level change rate is therefore positive, although small. If the observed change rate continues, the relative sea level at Copenhagen (in relation to land) will have increased by about 4.6 cm by 2100, compared to now. According to the IPCC, the modelled relative sea level (in relation to land) at Copenhagen will have increased about 45 cm by 2100, compared to now. A marked change in the relative sea-level increase is supposed to begin around 2020, in contrast to the previous slow sea-level increase recorded since 1889.

A few reflections might be appropriate here. The step change in relative sea level predicted for both sites (and many others) in 2020 appears implausible, and suggests that the modelled data is not capturing real-world dynamics.

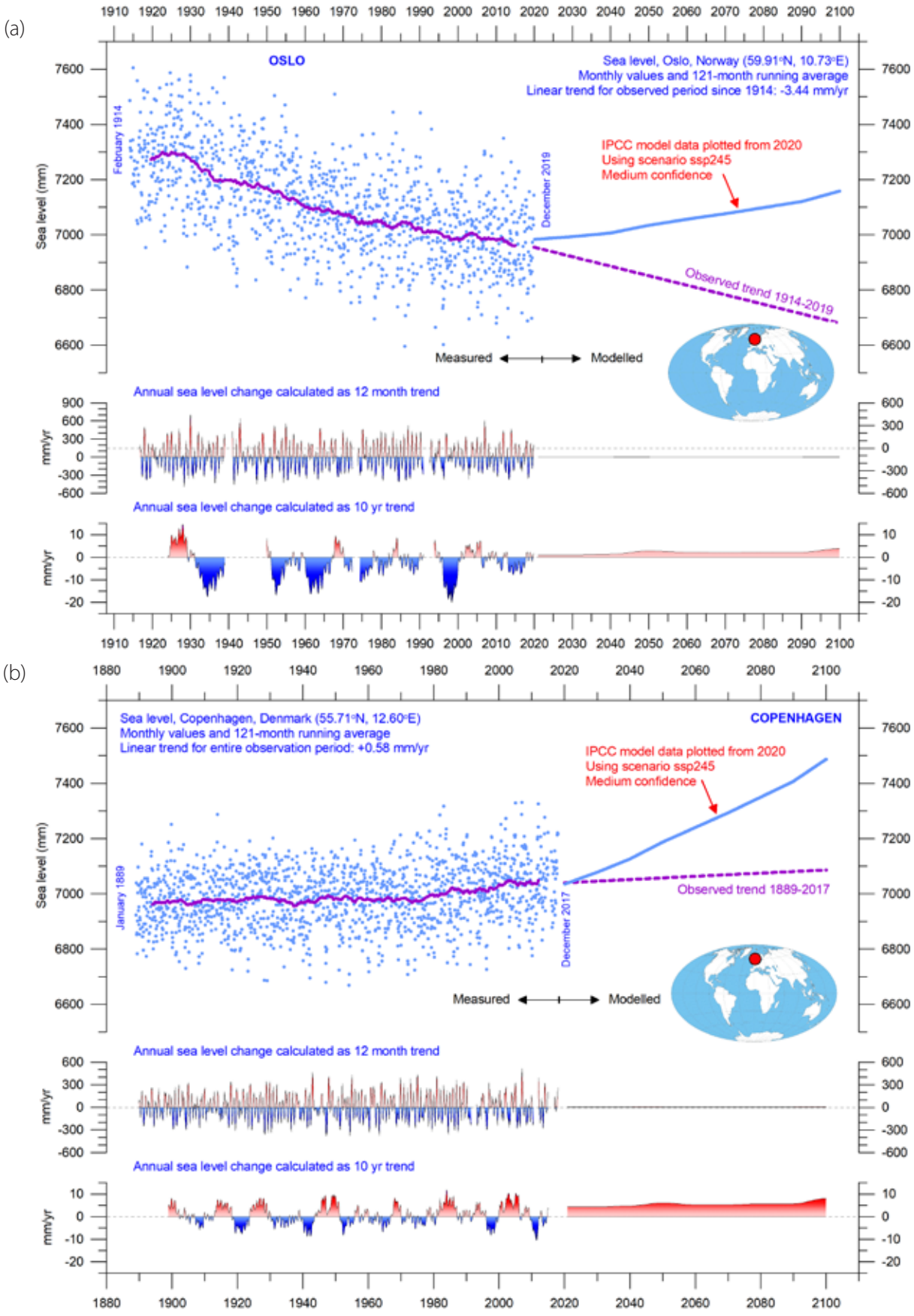

Figure 39: Observed and modelled sea level.

(a) Oslo and (b) Copenhagen. The blue dots are the individual monthly tide gauge observations (PSMSL Data Explorer) 1914–2019, and the purple line represents the running 121-month (ca. 10-year) average. The modelled data for the future is shown by a solid blue line 2020–2100, using the moderate SSP2–4.5 scenario (IPCC 2020). The two lower panels show the annual sea-level change, calculated for 1- and 10-year time windows, respectively. These values are plotted at the end of the interval considered.

6. Snow and ice

Global, Arctic and Antarctic sea ice extent

Figure 40 reveals constrasting developments in average sea-ice extent between the two poles. The modern Northern Hemisphere sea-ice trend towards smaller extent is clearly displayed by the blue graph, and so is the simultaneous increase of Southern Hemisphere sea-ice extent until 2016.

The Antarctic sea-ice extent decreased extraordinary rapidly during the Southern Hemisphere spring of 2016, much faster than in any

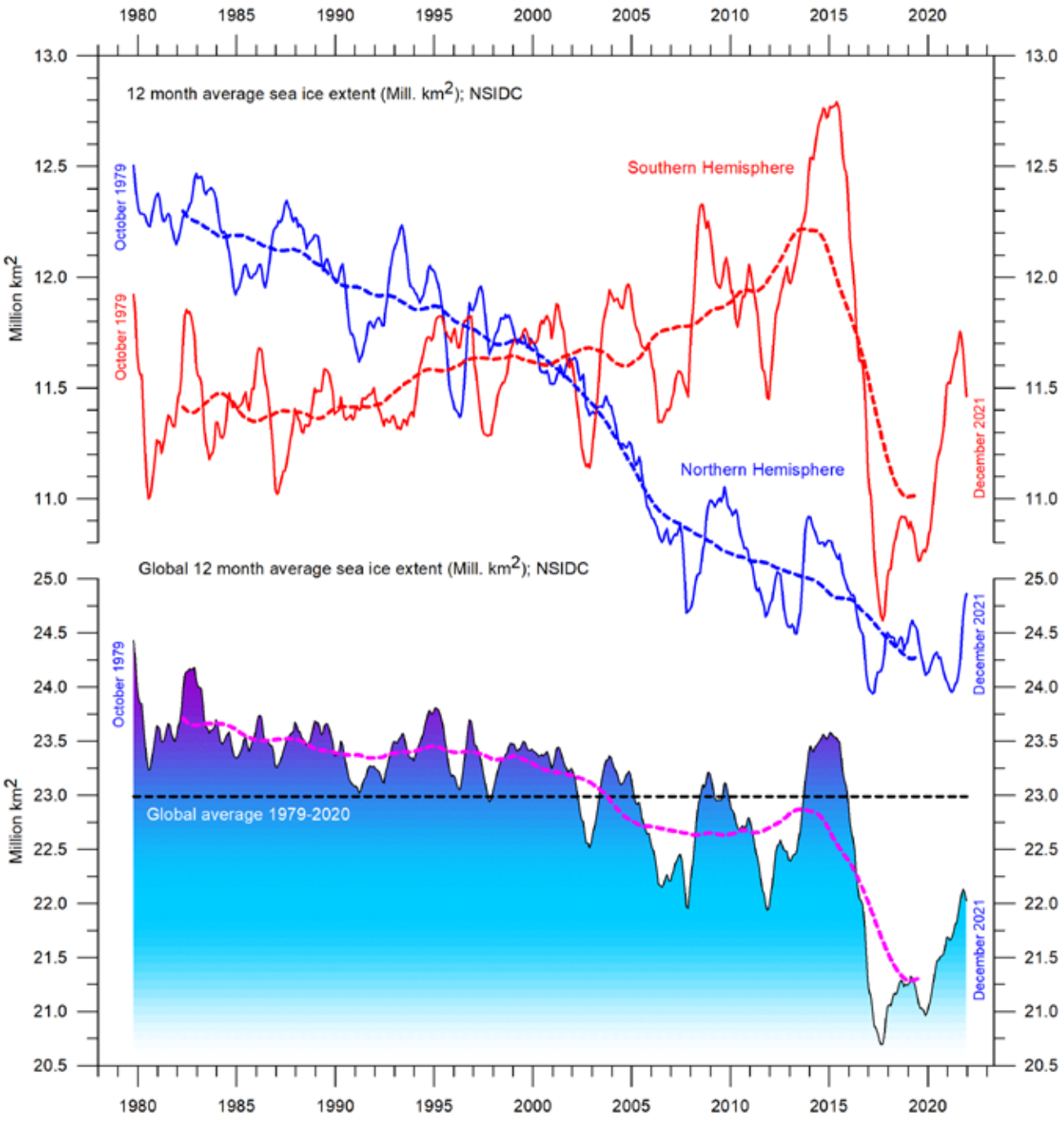

Figure 40: Global and hemispheric sea ice extent since 1979

12-month running means. The October 1979 value represents the monthly average of November 1978–October 1979, the November 1979 value represents the average of December 1978–November 1979, etc. The stippled lines represent a 61-month (ca. 5 years) average. The last month included in the 12-month calculations is shown to the right in the diagram. Data source: National Snow and Ice Data Center (NSIDC).

previous spring during the satellite era (since 1979). A strong retreat occurred in all sectors of the Antarctic, but was greatest in the Weddell and Ross Seas. In these sectors, strong northerly (warm) surface winds pushed the sea ice back towards the Antarctic continent. The background for the special wind conditions in 2016 has been discussed by various authors (e.g. Turner et.al. 2017 and Phys.org 2019) and appears to be a phenomenon related to natural climate variability.

The satellite sea-ice record is still short, and does not fully represent natural variations playing out over more than a decade or two. Nevertheless, it is instructive. The two graphs in Figure 40 reveal recurring variations superimposed on the overall trends. The Arctic sea ice is strongly influenced by a 5.3-year periodic variation, while the Antarctic sea ice has a periodic variation of about 4.5 years. Both these variations reached their minima simultaneously in 2016, which at least partly explains the simultaneous minimum in global sea-ice extent.

In the coming years, these variations may induce an increase in sea-ice extent at both poles, with an increase in the 12-month average global sea-ice extent as a possible result. In fact, such a development has already started for the Antarctic (Figure 40). For the Arctic, the average ice extent recently revealed signs of increasing (Figure 40). However, in the coming years, the minima and maxima for these variations will not occur synchronously, because of their different period length, and global minima (or maxima) may therefore in the coming years be less pronounced than in 2016.

The diagrams in Figure 41 illustrate the overall extent and thickness of the Arctic sea ice from end of 2020 to end of 2021, as published by the Danish Meteorological Institute.

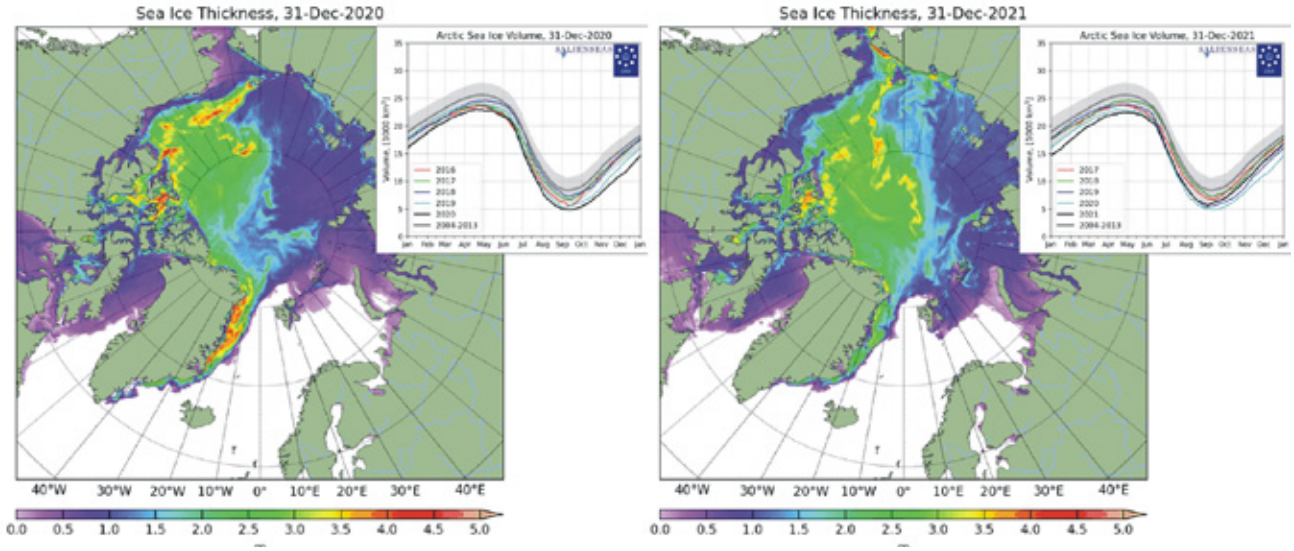

Figure 41: Arctic sea ice 2020 versus 2021

Arctic sea-ice extent and thickness 31 December 2020 (left) and 2021 (right) and the seasonal cycles of the calculated total arctic sea ice volume, according to the Danish Meteorological Institute (DMI). The mean sea ice volume and standard deviation for the period 2004–2013 are shown by grey shading in the insert diagrams.

Northern Hemisphere snow cover

Variations in global snow cover are mainly due to changes playing out in the Northern Hemisphere (Figure 42), where all the major land areas are located. The Southern Hemisphere snow cover is essentially controlled by the Antarctic Ice Sheet, and therefore relatively stable.

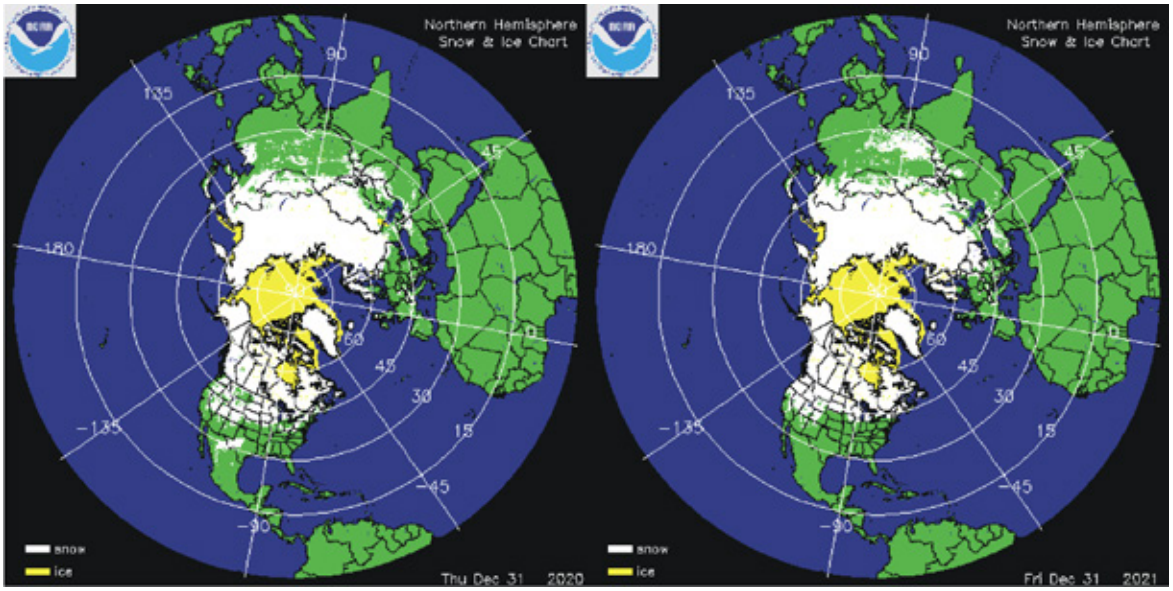

Figure 42: Northern hemisphere snow and sea ice

Snow cover (white) and sea ice (yellow) 31 December 2020 (left) and 2021 (right). Map source: National Ice Center (NIC).

The Northern Hemisphere snow cover exhibits large local and regional variations from year to year. However, the overall tendency (since 1972) is towards stable Northern-Hemisphere snow conditions, as illustrated by Figure 43.

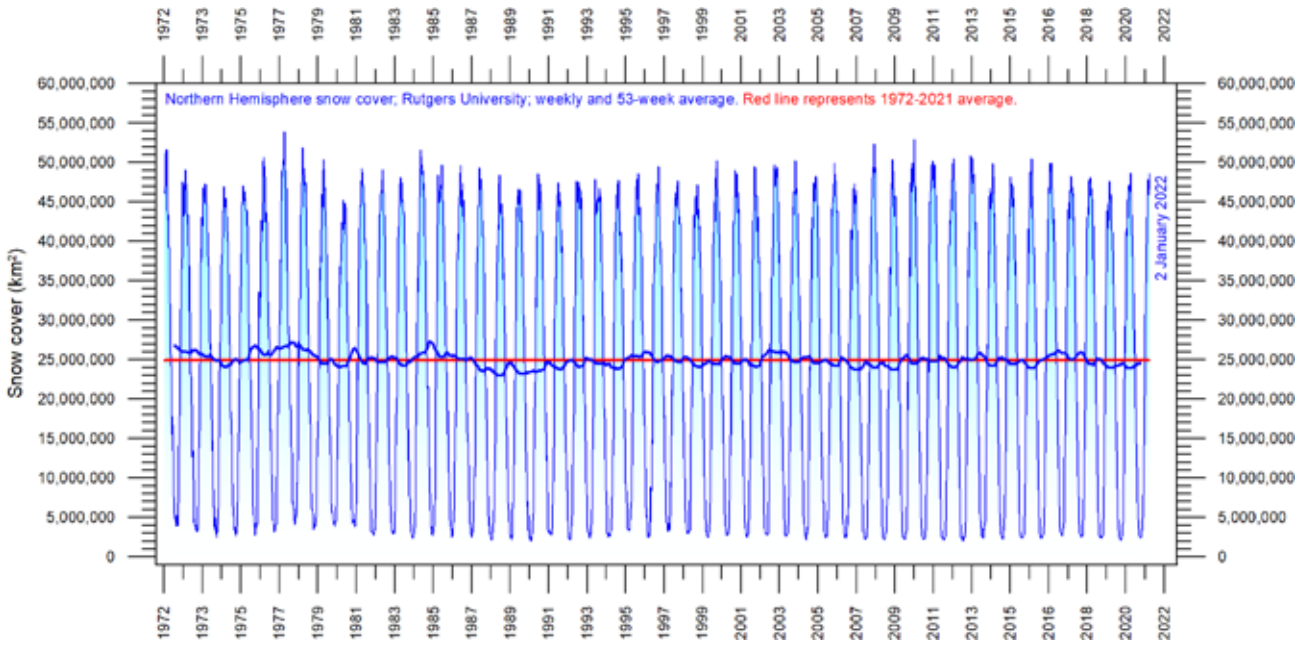

Figure 43: Northern hemisphere weekly snow cover since 1972

Source: Rutgers University Global Snow Laboratory. The thin blue line is the weekly data, and the thick blue line is the running 53-week average (approximately 1 year). The horizontal red line is the 1972–2020 average.

During the Northern Hemisphere summer, the snow cover usually shrinks to about 2,400,000 km^2 (principally controlled by the size of the Greenland Ice Sheet), and during the Northern Hemisphere winter the snow-covered area increases to about 50,000,000 km^2, representing no less than 33% of planet Earth's total land area.

Considering seasonal changes (Figure 44), the Northern Hemisphere snow cover during the autumn is slightly increasing, the mid-winter extent is basically stable, and the spring extent is slightly decreasing. In 2021, the Northern Hemisphere snow cover was close to the 1972–2020 average.

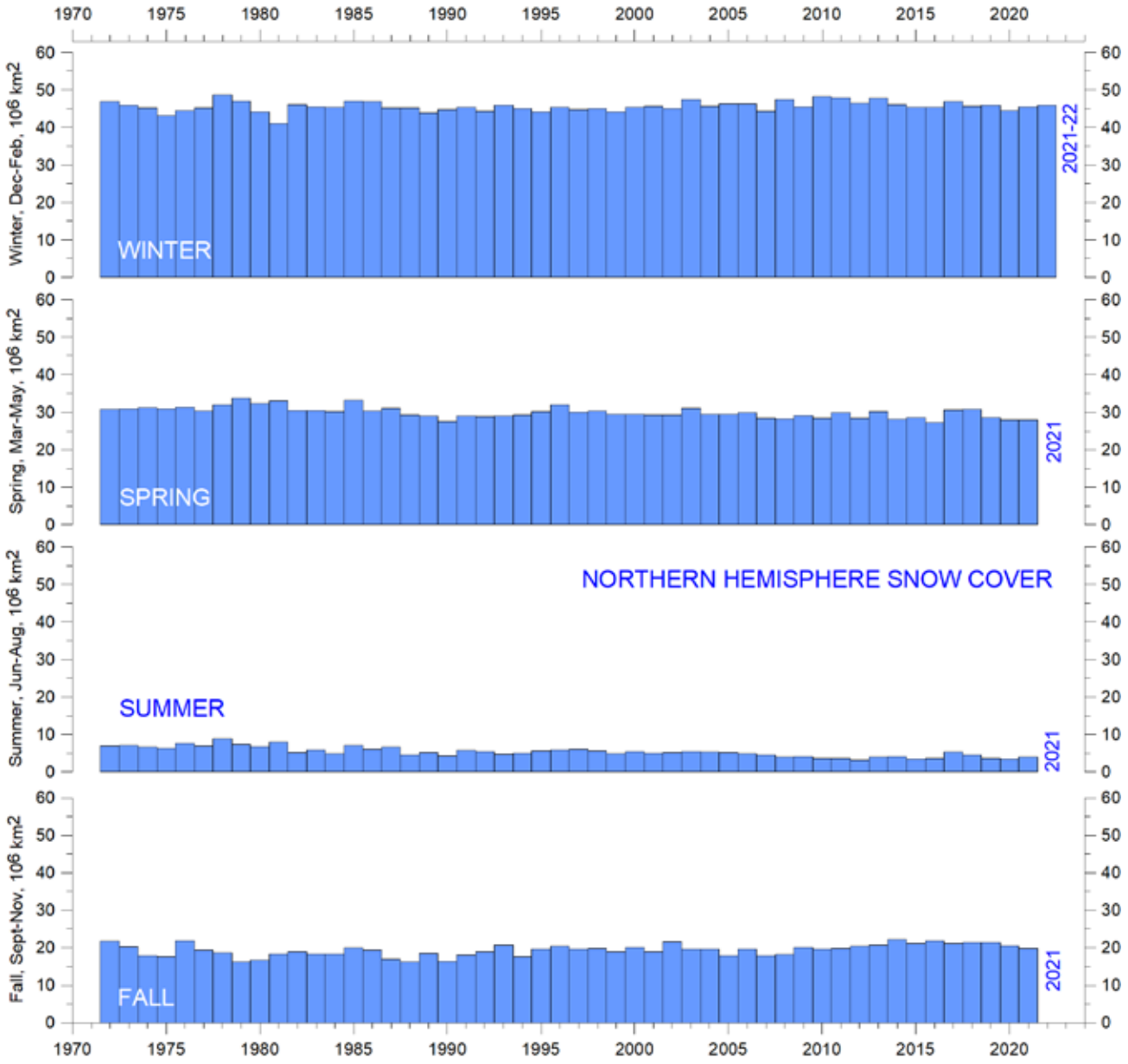

Figure 44: Northern Hemisphere seasonal snow cover since 1972

Data source: Rutgers University Global Snow Laboratory.

7. Storms and wind

Accumulated cyclone energy

Accumulated cyclone energy (ACE) is a measure used by the National Oceanic and Atmospheric Administration (NOAA) to express the activity of individual tropical cyclones and entire tropical cyclone seasons. ACE is calculated as the square of the wind speed every 6 hours, scaled by a factor of 10,000 for usability. It has units of 10^4 knots^2. The ACE of a season is the sum of the ACE for each storm and encapsulates the number, strength, and duration of all the tropical storms in the season.

The damage potential of a hurricane is proportional to the square or cube of the maximum wind speed, and ACE is therefore not only a measure of tropical cyclone activity, but also a measure of the damage potential of an individual cyclone or a season. Existing records (Figure 45) do not suggest any abnormal cyclone activity in recent years.

The ACE data since 1970 display a variable pattern over time (Figure 45), but without any clear trend. This is true globally and for the separate Northern- and Southern Hemisphere data (panels in Figure 45). A Fourier analysis (not shown here) shows a significant period of about 3.6 years in the ACE data, and furthermore sug-

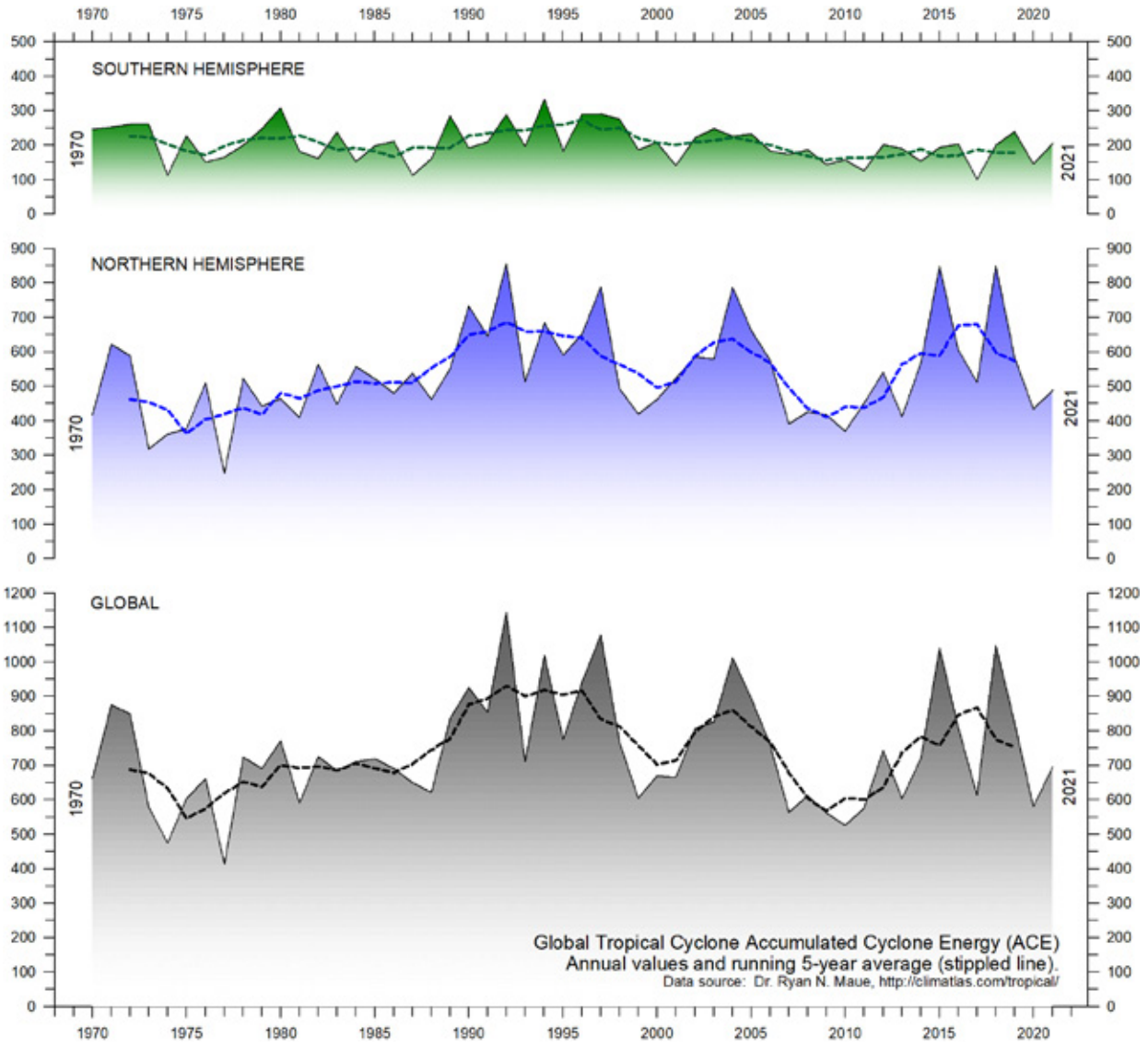

Figure 45: Annual global accumulated cyclone energy

Source: Ryan Maue.

gests the existence of a 11.5-year period. However, the data series is still too short to draw firm conclusions.

The period 1989–1998 was characterised by high values; other peaks were seen 2004, 2015 and 2018, while the periods 1973–1988, 1999–2003 and 2006–2014 had low values. The peaks in 1997/98 and 2016 coincide with strong El Niño events in the Pacific Ocean (Figure 23). The ACE data and ongoing cyclone dynamics are detailed in Maue (2011). The Northern Hemisphere ACE values (central panel in Figure 45) dominates the global signal (lower panel in Figure 45) and therefore show similar peaks and lows as displayed by the global data, without any clear trend for the entire observational period. The main Northern Hemisphere cyclone season is June–November. The Southern Hemisphere ACE values (upper panel in Figure 45) are generally lower than for the Northern Hemisphere, and the main cyclone season is December–April.

The Atlantic Oceanographic and Meteorological Laboratory ACE data series goes back to 1850 (Figure 46). A Fourier analysis (not shown) shows the ACE series to be strongly influenced by a periodic variation of about 60 years' duration. Since 2002, the Atlantic ACE series has displayed an overall declining trend, but with large interannual variations. The North Atlantic hurricane season often shows above-average activity when La Niña conditions are present in Pacific during late summer (August–October), as was the case in 2017 (Johnstone and Curry, 2017).

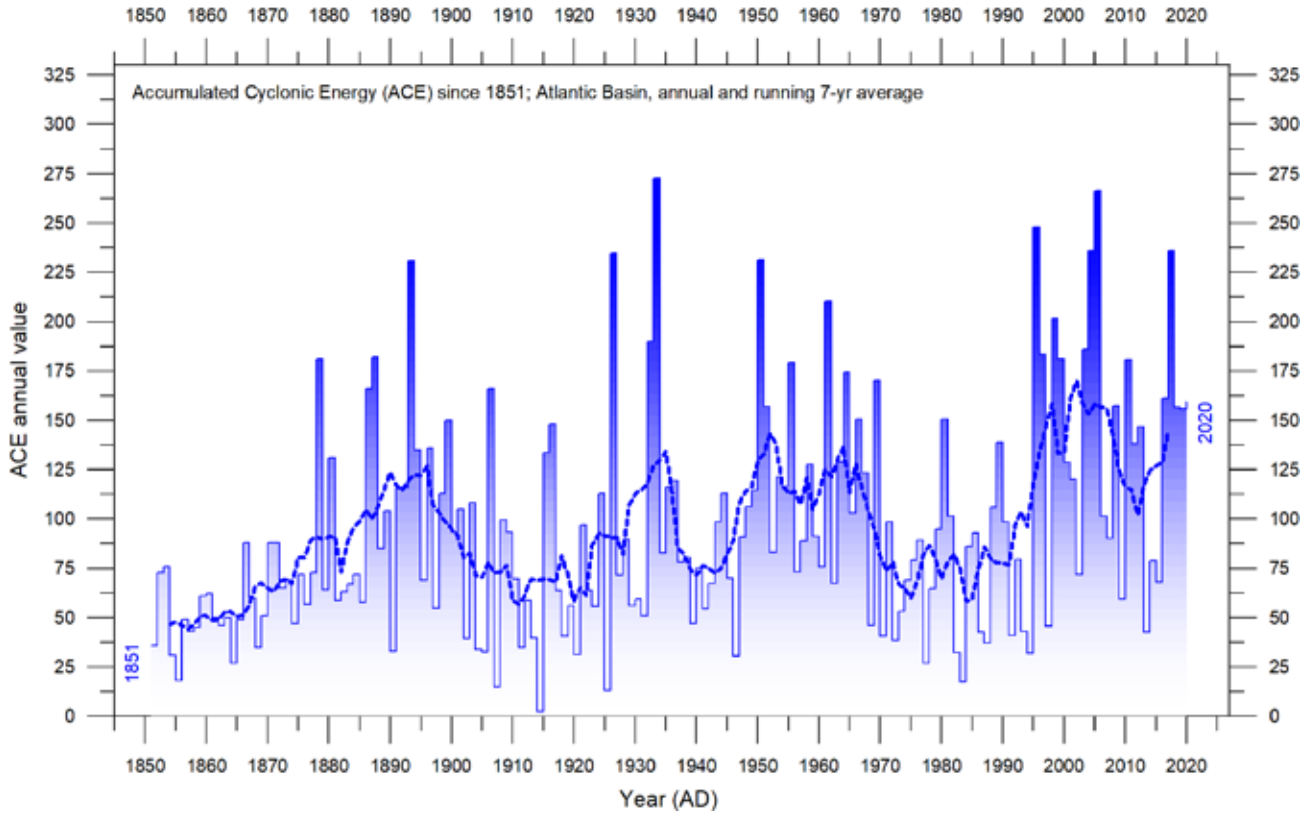

Figure 46: Atlantic Basin ACE since 1851

Thin lines show annual ACE values, and the thick line shows the running 7-year average. Data source: Atlantic Oceanographic and Meteorological Laboratory (AOML), Hurricane Research Division. Please note that these data are not yet updated beyond 2020.

Other storm and wind observations

The number of Continental United States Hurricane landfalls is shown in Figure 47. Over the observational period, this data series shows considerable variations from year to year, but it is not possible to detect any clear trend over time. A Fourier analysis (not shown here) shows this annual data series to be characterised by two statistically significant periods, about 3.2 and 4.9 years long, respectively.

Insight into changes of prevailing wind conditions may also be obtained from the inspection of observations carried out at particularly wind-exposed coastal meteorological stations. One example from north-west Europe is Lista Lighthouse in southernmost Norway. This sits on an exposed cape at the extreme southwestern edge of the mainland of Norway, and is thus well suited to register wind conditions in the adjoining North Sea and the European sector of the North Atlantic. Lista Lighthouse has a monthly wind record going back to January 1931, as displayed in Figure 48. At this location, the peak wind strengths were recorded shortly after World War II, and have since declined somewhat, to some degree reflecting the overall development displayed by the number of Continental United States Hurricane landfalls (Figure 47), on the opposite shore of the North Atlantic.

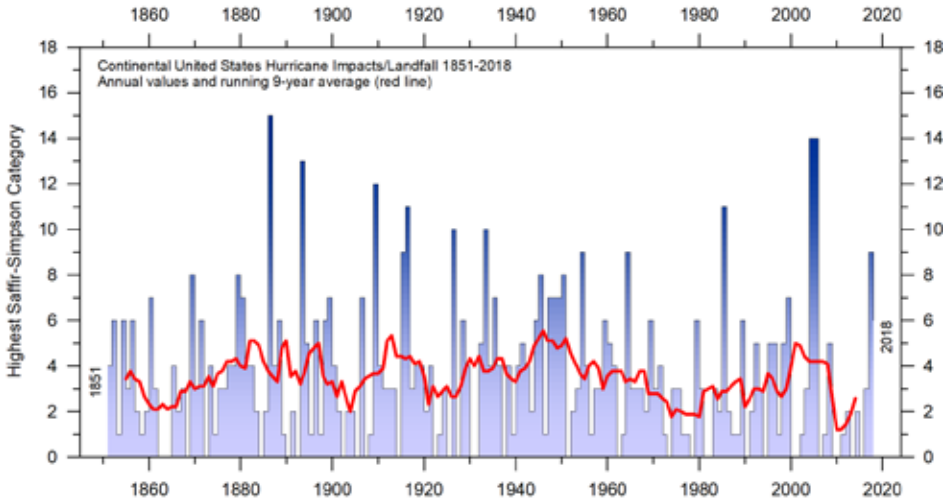

Figure 47: Hurricane landfalls in the continental United States 1851–2018

The highest Saffir-Simpson Hurricane Scale impact in the United States is based upon estimated maximum sustained surface winds produced at the coast. Data source: Hurricane Research Division, NOAA. Please note that this data series is not yet updated beyond 2018.

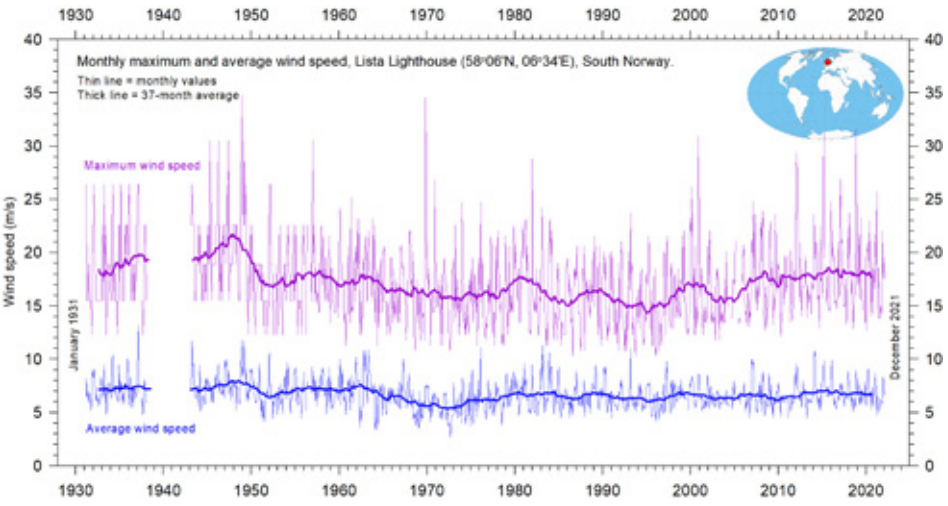

Figure 48: Monthly maximum and average wind speed since January 1931 measured at Lista Lighthouse, South Norway

Lista Lighthouse is situated on an exposed cape located at the extreme southwestern edge of mainland Norway, in a position to register wind conditions in the adjoining North Sea and the European sector of the North Atlantic. Data source: SeKlima.

8. Written references

Carter R.M., et al. 2014. *Commentary and Analysis on the Whitehead & Associates 2014 NSW Sea-Level Report.* Policy Brief, NIPCC, 24. September 2014, 44 pp. http://climatechangereconsidered.org/wp-content/uploads/2014/09/NIPCC-Report-on-NSW-Coastal-SL-9z-corrected.pdf.

Chylek, P., et al. 2010. Twentieth century bipolar seesaw of the Arctic and Antarctic surface air temperatures. *Geophysical Research Letters*, 37, L08703, doi:10.1029/2010GL042793.

Holgate, S.J. 2007. On the decadal rates of sea level change during the twentieth century. *Geophysical Research Letters*, 34, L01602, doi:10.1029/2006GL028492.

Johnstone, J. and Curry, J. 2017. *Causes and Predictability of the Exceptionally Active 2017 Atlantic Hurricane Season*. Climate Forecast Applications Network (CFAN), 9 pages. https://curryja.files.wordpress.com/2017/11/hurricane_review_2017-final.pdf.

Maue, R.L. 2011. Recent historically low global tropical cyclone activity. *Geophysical Research Letters*, Vol. 38, L14803, doi:10.1029/2011GL047711.

Roemmich, D. and J. Gilson, 2009. The 2004–2008 mean and annual cycle of temperature, salinity, and steric height in the global ocean from the Argo Program. *Progress in Oceanography*, 82, 81–100.

Turner J. et al. 2017. Unprecedented springtime retreat of Antarctic sea ice in 2016. *Geophysical Research Letters*, Vol.44(13), p. 6868–6875. https://doi.org/10.1002/2017GL073656.

Vignudelli S. et al. 2019. Satellite altimetry measurements of sea level in the coastal zone. *Surveys in Geophysics, Vol.* 40, p. 1319–1349. https://link.springer.com/article/10.1007/s10712-019-09569-1.

9. Links to data sources

(All accessed January–February 2022)

AMO, Earth System Research Laboratory, NOAA, USA: https://www.esrl.noaa.gov/psd/data/timeseries/AMO/.

Atlantic Oceanographic and Meteorological Laboratory, Hurricane Research Division: http://www.aoml.noaa.gov/hrd/tcfaq/E11.html.

Colorado Center for Astrodynamics Research: http://sealevel.colorado.edu/.

Danish Meteorological Institute (DMI): http://ocean.dmi.dk/arctic/icethickness/thk.uk.php.

Earth System Research Laboratory (ESRL): https://www.esrl.noaa.gov/psd/map/clim/olr.shtml.

SeKlima: https://seklima.met.no/observations/.

GISS temperature data: https://data.giss.nasa.gov/gistemp/.

Global Marine Argo Atlas: http://www.argo.ucsd.edu/Marine_Atlas.html.

Goddard Institute for Space Studies (GISS): https://www.giss.nasa.gov/.

HadCRUT temperature data: http://hadobs.metoffice.com/.

Hurricane Research Division, NOAA: http://www.aoml.noaa.gov/hrd/tcfaq/E23.html.

National Ice Center (NIC). http://www.natice.noaa.gov/pub/ims/ims_gif/DATA/cursnow.gif.

National Snow and Ice Data Center (NSIDC): http://nsidc.org/data/seaice_index/index.html.

NCDC temperature data: https://www.ncdc.noaa.gov/monitoring-references/faq/.

Ocean temperatures from Argo floats: http://www.argo.ucsd.edu/.

Oceanic Niño Index (ONI): http://www.cpc.ncep.noaa.gov/products/analysis_monitoring/ensostuff/ensoyears.shtml.

Outgoing long wave radiation (OLR): https://www.esrl.noaa.gov/psd/map/clim/olr.shtml.

PDO, NOAA Physical Sciences Laboratory: https://psl.noaa.gov/pdo/.

Permanent Service for Mean Sea Level: http://www.psmsl.org/.

Phys.org 2019: https://phys.org/news/2019-01-antarctica-sea-ice-climate.html.

Plymouth State Weather Center: http://vortex.plymouth.edu/sfc/sst/.

PSMSL Data Explorer: http://www.psmsl.org/data/obtaining/map.html.

Rutgers University Global Snow Laboratory: http://climate.rutgers.edu/snowcover/index.php.

RSS temperature data: http://www.remss.com/measurements/upper-air-temperature.

Sea level from satellites: https://sealevel.colorado.edu/data/2020rel1-global-mean-sea-level-seasonal-signals-retained.

Sea level from tide-gauges: http://www.psmsl.org/data/obtaining/map.html.

Sea level modelled: IPCC AR6 Sea Level Projection Tool: https://sealevel.nasa.gov/data_tools/17.

Sea ice extent Danish Meteorological Institute (DMI): http://ocean.dmi.dk/arctic/icethickness/thk.uk.php.

Southern Oscillation Index (SOI): http://crudata.uea.ac.uk/cru/data/soi/.

Maue ACE data: climatlas.com/tropical/.

UAH temperature data: http://www.nsstc.uah.edu/data/msu/v6.0/tlt/uahncdc_lt_6.0.txt.

Review process

GWPF publishes papers in a number of different formats, with a different review process pertaining to each.

- Our flagship long-form GWPF Reports are all reviewed by our Academic Advisory Council.
- GWPF Briefings and Notes are shorter documents and are reviewed internally and/or externally as required.

Part of the function of the review process is to ensure that any materials published by the GWPF are of a proper academic standard, and will serve the GWPF's educational purpose. As a charity, we recognise that educational material should provide any reader the opportunity to understand, and explore different perspectives on a subject.

This means that, for most publications, we also invite an external review from a party who we would expect to take a different view to the publication's author. We offer to publish any substantive comments alongside the main paper, provided we are satisfied they will enhance the educational experience of the reader. In this way, we hope to encourage open and active debate on the important areas in which we work.

This enhanced review process for GWPF papers is intended to take the content and analysis beyond a typical review for an academic journal:

- More potential reviewers can be involved
- The number of substantive comments will typically exceed journal peer review, and
- The identity of the author is known to the potential reviewers.

As an organisation whose publications are sometimes the subject of assertive or careless criticism, this review process is intended to enhance the educational experience for all readers, allowing points to be made and considered in context and observing the standards required for an informed and informative debate. We therefore expect all parties involved to treat the reviews with the utmost seriousness.

Final responsibility for publication rests with the Chairman of the Trustees and the GWPF Director. But in every case, the views expressed are those of the author. GWPF has never had any corporate position beyond that dictated by its educational objectives.

About the Global Warming Policy Foundation

People are naturally concerned about the environment, and want to see policies that enhance human wellbeing and protect the environment; policies that don't hurt, but help.

The Global Warming Policy Foundation (GWPF) is committed to providing a platform for educational research and informed debates on these important issues.

In order to make progress and advance effective policy assessments, it is essential to cultivate a culture of open debate, tolerance and learning.

Our aim is to raise standards in learning and understanding through rigorous research and analysis, to help inform a balanced debate amongst the interested public and decision-makers.

We aim to create an educational platform on which common ground can be established, helping to overcome polarisation and partisanship. We aim to promote a culture of debate, respect, and a hunger for knowledge.

RECENT GWPF REPORTS

16	Montford	Unintended Consequences of Climate Change Policy
17	Lewin	Hubert Lamb and the Transformation of Climate Science
18	Goklany	Carbon Dioxide: The Good News
19	Adams	The Truth About China
20	Laframboise	Peer Review: Why Scepticism is Essential
21	Constable	Energy Intensive Users: Climate Policy Casualties
22	Lilley	£300 Billion: The Cost of the Climate Change Act
23	Humlum	The State of the Climate in 2016
24	Curry et al.	Assumptions, Policy Implications and the Scientific Method
25	Hughes	The Bottomless Pit: The Economics of CCS
26	Tsonis	The Little Boy: El Niño and Natural Climate Change
27	Darwall	The Anti-development Bank
28	Booker	Global Warming: A Case Study in Groupthink
29	Crockford	The State of the Polar Bear Report 2017
30	Humlum	State of the Climate 2017
31	Darwall	The Climate Change Act at Ten
32	Crockford	The State of the Polar Bear Report 2018
33	Svensmark	Force Majeure: The Sun's Role in Climate Change
34	Humlum	State of the Climate 2018
35	Peiser (ed)	The Impact of Wind Energy on Wildlife and the Environment
36	Montford	Green Killing Machines
37	Livermore	Burnt Offering: The Biomess of Biomass
38	Kelly	Decarbonising Housing: The Net Zero Fantasy
39	Crockford	The State of the Polar Bear Report 2019
40	Darwall	The Climate Noose: Business, Net Zero and the IPCC's Anticapitalism
41	Goklany	The Lancet Countdown on Climate Change: The Need for Context
42	Humlum	The State of the Climate 2019
43	Alexander	Weather Extremes: Are They Caused by Global Warming?
44	Constable	Hydrogen: The Once and Future Fuel?
45	Kessides	The Decline and Fall of Eskom: A South African Tragedy
46	Goklany	Impacts of Climate Change: Perception and Reality
47	Constable	A Little Nudge with a Big Stick
48	Crockford	The State of the Polar Bear Report 2020
49	Alexander	Weather Extremes in 2020
50	Humlum	The State of the Climate 2020
51	Humlum	The State of the Climate 2021

For further information about the Global Warming Policy Foundation, please visit our website at www.thegwpf.org.
The GWPF is a registered charity, number 1131448.